MAESTRÍA DE INGENIERÍA ELÉCTRICA

TESIS DE GRADO

Optimal Operation of Active Distribution Networks

Simón Sepúlveda García

Pereira
March 30, 2023

Optimal Operation of Active Distribution Network

Por:
Simón Sepúlveda García

Tesis de grado para optar al titulo de Magister en Ingeniería Eléctrica

Dirigida por:
Alejandro Garcés Ruíz

Maestría en Ingeniería Eléctrica
Universidad Tecnológica de Pereira
March 30, 2023

Abstract

This document presents a generic Optimal Power Flow Formulation (OPF) for operating Active Distribution networks during grid-connected and grid-islanded modes. The optimization model is intended to be executed in real-time, considering the effect of droop controls. Hence, fast convergence and global optimum are required to guarantee the grid's optimal operation during these two operation modes. For this reason, the mixed integer non-linear programming model is relaxed into a convex optimization model. Several approaches are discussed to evaluate the convergence and computation time performance. The results demonstrate that the Wirtinger linearization presents the best performance; furthermore, the optimization model guarantees a proper and safe operation while minimizing operations costs.

Acknowledgement

This Master's Thesis could not have been finished without the affection and lovely patience of my girlfriend Natalia, who lovingly pushed me through the most difficult times. Furthermore, I would like to specially thanks Alejandro Garcés Ruíz and Juan José Mora for their patience, guidance, and recommendations.

This Master's Thesis is a result of project Integra2023, code 111085271060,contract 80740-774-2020, funded by the Ministry of Science, Technology and Innovation (Minciencias)

Contents

1 Introduction **10**

1.1 Motivation 10

1.2 State of the art 11

1.3 Objectives 14

1.3.1 General objective 14

1.4 Contributions 15

1.4.1 List of Publications 15

1.5 Document organization 17

2 Hierarchical Control in Active Distribution Networks **19**

2.1 Level-zero and primary control 20

2.1.1 Level-zero control 20

2.1.2 Primary control 23

2.2 Secondary control 25

2.3 Tertiary control 26

2.4 Operation modes 27

2.4.1 Grid-connected operation 28

2.4.2 Grid islanded operation 28

3 Optimal Operation in Active Distribution Networks **30**

3.1 Model of the grid 30

3.2 Model of distributed energy resources 33
3.2.1 Distributed generators 33
3.2.2 Model of solar panels 34
3.2.3 Model of wind turbines 34
3.2.4 Model of energy storage systems 35
3.3 Technical constraints 36
3.4 Balanced case (single-phase equivalent) 37
3.5 Three-phase case 39

4 Convex approximations **42**
4.1 Second-order cone approximation 42
4.2 Sequential convex optimization 44
4.3 Wirtinger calculus 45
4.4 Effect of the frequency 48

5 Results **50**
5.1 Methodological framework 50
5.2 Variation of the Y_{bus} as function of the frequency 51
5.3 Single phase case 56
5.3.1 Connected mode 57
5.3.2 Islanded mode 57
5.3.3 Generic operation 59
5.3.4 Extension to meshed grids 62
5.4 Three-Phase Case 64

6 Conclusions, discussion and future work **67**
6.1 Future work 68
6.2 Applicability to the Colombian Case 69

Apendices **73**

A Data for single phase case **74**

B Data for three-phase case **77**

List of Tables

1.1 Publications about optimal operation of Active Distribution Networks . . . 13

2.1 Type of control for layer-zero according to converters' functionality (Rocabert et al., 2012) . . . 21

5.1 General results of the proposed optimization model in others test systems. . . . 54

5.2 Computation Times for Different test systems and mean r/x ratio . . . 54

5.3 Value of the objective function for different operation modes . 63

A.1 BESS information . . . 75

A.2 DGs information . . . 75

A.3 PV units data . . . 75

A.4 BESS information . . . 75

A.5 DGs information . . . 76

A.6 PV units data . . . 76

B.1 BESS information . . . 78

B.2 DGs information . . . 78

B.3 PV units data . . . 78

List of Figures

1.1 Document organization 18

2.1 Schematic representation of an active distribution network (Figure taken from (Sepulveda et al., 2022b)). 19

2.2 Hierarchical control of active distribution networks, including typical time window for each control 21

2.3 Example of grid following converters and its internal control (Vector Oriented Control, VOC). 22

2.4 Schematic representation of inverse grid-forming converters . 23

2.5 Primary control: conventional droop controls (above) and inverse droop controls (below) 24

2.6 Dynamic behavior for each control layer (Adapted from (Rios and Garces, 2022)) 25

2.7 Operation modes of active distribution networks 27

3.1 Nodal (and equivalent) representation of a grid 30

4.1 Representation of a Second Order Cone 44

4.2 Representation of a linear approximation around and operation point. 47

5.1 Irradiance in Riohacha for February First 51

5.2 Temperature in Riohacha for February First 51

5.3 Wind speed in Riohacha for February First 52

5.4 Norm of p_{km} with respect the r/x ratio 53
5.5 Convergence for different benchmarks. 54
5.6 Variation of the Y_{bus} for the 23,33 and 34 nodes test systems. 55
5.7 Variation of the Y_{bus} for the 69 and 100 nodes test systems. . 55
5.8 Power dispatch during full Grid-Connected (GC) mode. . . . 58
5.9 BESS energy during full Grid-Connected (GC) mode. 58
5.10 Power dispatch during full Grid-Islanded (GI) mode. 59
5.11 BESS energy during full Grid-Islanded (GI) mode. 60
5.12 Power dispatch for the Generic Mode with two disconnections from the main grid. 61
5.13 BESS energy for the generic mode with two disconnections from the main grid. 61
5.14 Frequency response during the different operation schemes . . 62
5.15 Voltage variation at the slack node during operation horizon . 62
5.16 Power dispatch for CIGRE meshed grid during GI mode. . . 63
5.17 Frequency response for CIGRE meshed grid. 64
5.18 Power dispatch for GI operation three phase 25 nodes 65
5.19 Frequency response for 25 nodes three phase benchmark during GI mode of operation 65
5.20 Voltage profiles at time t=0 for three phase GI mode of operation 66
5.21 Voltage profiles at time t=19 for three phase GI mode of operation. 66

A.1 Load curve for a daily operation 74

B.1 Load curve for a daily operation 77

Chapter 1

Introduction

1.1 Motivation

Distribution networks are vital infrastructures connecting the bulk power system with the customers. These networks have grown organically throughout the 20th century to reach a point where they require updating. Nowadays, distribution networks have gained increasing interest due to the penetration of distributed generators and the increasing presence of communication technologies, automation, and constant monitoring through supervisory control and data acquisition systems (SCADAs). Thus, the Active Distribution Network (ADN) corresponds to an evolution of the networks that incorporates the technologies listened to above. ADNs may have better performance by reducing power losses, improving the profits of Distribution System Operators (DSO), and enhancing resilience and security. In order to accomplish these advantages, it is necessary to develop supervisory control algorithms such as the Optimal Power Flow (OPF) (Groppi et al., 2021; Mishra et al., 2021).

The optimal power flow is the generic name for different optimization models in power systems operation, including the effect of the network. The OPF must also include the frequency effect in the nodal admittance matrix and the droop controls in the primary control for isolated operation. This problem is called dynamic optimal power flow (DOPF) and is more complex than the conventional OPF. Notice that different problems are named DOPF in the literature (Abdi et al., 2017); in this case, it is defined as an OPF that includes the effect of the primary control and the frequency.

1.2 State of the art

Active Distribution Networks (ADNs) emerge from conventional distribution networks, allowing the integration of distributed energy resources (DER) such as renewable power generation and energy storage devices (Costa et al., 2020). These new grids may enhance reliability, with high penetration of communication technologies, automatization, and the ability of consumers to become *prosumers*[1] (Kryonidis et al., 2021).

An ADN could operate either in grid-connected or grid-islanded mode. The latter is possible when distribution generator units provide frequency and voltage support after a disturbance (or intentional disconnection) from the primary grid (Dragičević et al., 2021). During Grid-Islanded (GI) mode, DERs must cease their constant generation and regulate frequency and voltage. The primary control stabilizes those variables, and the secondary control carries them to the values found by executing the tertiary control.

These layers form what is known as hierarchical control. The tertiary layer (on which this study focuses) defines new set-points for renewable and storage devices using optimization models such as the optimal power flow (OPF) (Abdi et al., 2017). In addition to the OPF, a combination of load shedding and generation management is required when the total amount of generation is lower than the total demand (i.e., the network has a generation deficit). This operation mode is a challenge since it must include generation and demand-side management, considering the effect of the primary control on the frequency and power-sharing (Guerrero et al., 2011). The optimization model must be fast enough to operate in real-time; hence, a convex optimization model is desirable in these circumstances; however, the main equations of the problem are non-convex (Lavaei and Low, 2012).

The optimal power flow problem has been extensively studied for the tertiary layer. Modern-day approaches include semidefinite programming (Gan and Low, 2014)(Huang et al., 2022a), conic optimization (especially second order-cone) (Montoya et al., 2020; Yuan and Hesamzadeh, 2018), quadratic programming (Bedoya et al., 2019) and linear approximations (Ramirez et al., 2021; Wu et al., 2017) (see (Molzahn and Hiskens, 2019) for a complete review of these approaches). These relaxations have a theoretical and practical advantage because convexity ensures global optimum and convergence in adequate computation times. Other approaches, such as

[1] A prosumer is an electric customer who generates electricity and sells excess back to the utility.

meta-heuristics and artificial intelligence-based methods, have also been proposed in the literature (see, for example, (Capitanescu, 2016) for a complete review). However, meta-heuristics have been discouraged in the scientific community due to their lack of mathematical rigor (Sorensen, 2015).

Optimal power flow models are usually designed for the grid-connected operation mode, where a slack bus fixes voltage and frequency. Nevertheless, during a grid-islanded operation mode, there is no presence of a slack bus, and all (or some) of the distributed generators must cease the constant power generation to follow demand variations to match the load consumption; otherwise, the frequency and voltage will deviate from their nominal value (Kreishan and Zobaa, 2021). For these reasons, several proposals regarding the formulation of power flow have been proposed in the specialized literature. For instance, (Mumtaz et al., 2016) proposes a modified version to calculate the Power Flow including droop controllers, (Bravo-López et al., 2021) proposed a Newton-Raphson Version that included droop controllers, the centroid of frequency and the inclusion of the frequency inside the Y_{bus}, (Díaz et al., 2016) extended the classical Backward Forward Sweep algorithm for stand-alone microgrids Grids, (Abdelaziz et al., 2013) proposed a Newton-trust region method to solve the power flow in isolated microgrids taking into account Droop controlled nodes, PV nodes, and PQ nodes. Most of these versions for calculating the power flow are hardly extensible to optimal power flow applications.

For the optimal operation of Grid Islanded, several methods have been proposed. For instance, (Ja'afreh et al., 2022) proposed a heuristic method that uses (Mumtaz et al., 2016) to operate isolated microgrids while maximizing the total amount of load coverage. (Olivares et al., 2014) Proposed an MINLP mathematical formulation of the energy management of isolated microgrids. However, decomposed the resulting MINLP into two sub-problems, a reduced MILP problem and a NLP problem, to obtain faster solutions than those obtained for commercial solvers of MINLP. The problem with this formulation is that they do not use droop controls to incorporate (and maintain the frequency between a stable range). (Alqunun et al., 2020) proposed a MILP problem to operate a microgrid during connected mode and to secure islanding operation during the islanded mode. The main problem of this proposal is not including droop controls (and, respectively, the incorporation of the frequency) into the optimization problem to secure and maintain a safe range of operation of voltage and frequency. (Hemmatpour et al., 2016) proposed a Heuristic method to reconfigure (in real-time) isolated radial microgrids in order to minimize the loss of load while taking into account the

grid and generator constraints (droop control). (Maulik and Das, 2018) proposed an optimization model for the optimal operation of droop-controlled islanded microgrids employing heuristic methods (fuzzified particle swarm optimization) for the optimal selection of droop settings of dispatchable distributed generation (DG) units to reduce operating costs and greenhouse emissions. (Liu et al., 2019) proposed a meta-heuristic method for the OPF in grid-islanded mode and handled the stochastic nature of DGs and loads by employing Monte Carlo Simulations.

(Vergara et al., 2019a) proposed an MINLP problem employing the Branch Flow Model Equations (BFM) to handle the optimal Operation of Droop Controlled Islanded microgrids and approximated it into a MISOC. (Vergara et al., 2020) proposed an MINLP problem employing the BFM equations and approximating it into a MILP problem using complex piecewise functions. The main problem of the Branch Flow Model Equations is that these equations only apply to radial grids; hence, those proposals need to be validated for meshed grids. Finally, since a typical day could arise, either Grid Connected (GC) Operation or Grid Islanded (GI) Operation, it would be beneficial to propose a model that can operate in both operation modes. However, only a few models have been proposed in the specialized literature. For instance, (Vergara et al., 2019b) proposed an MINLP problem for the generic optimal power flow employing BFM model equations (not being applicable for meshed grids), and (Alqunun et al., 2020) presented a generic optimization model without considering droop controls (and hence, not including the frequency into the optimization problem); a summary of the most relevant articles that addressed either the problem of grid-islanded operation is given in Table 1.1.

Table 1.1: Publications about optimal operation of Active Distribution Networks

Articles	Approach	Convex	Generic OPF	meshed grid application	Droop Scheme	Inverse droop	Load shedding
(Vergara et al., 2019a)	MISOC	●	◐	○	●	○	●
(Vergara et al., 2020)	MILP	●	◐	○	●	○	●
(Vergara et al., 2019b)	MISOC	●	●	○	●	○	●
(Ramirez et al., 2021)	LP	●	◐	●	○	○	○
(Olivares et al., 2014)	MILP/NLP	◐	◐	●	○	○	○
(Bassey et al., 2021)	LP	●	◐	●	●	○	○
(Alqunun et al., 2020)	MILP	●	●	●	○	○	●
(Hemmatpour et al., 2016)	H	○	◐	○	●	○	●
(Maulik and Das, 2018)	H	○	◐	●	●	○	○
(Ja'afreh et al., 2022)	H	○	◐	●	●	◐	◐
This approach	MILP/MIQP	●	●	●	●	●	●

Here we could observe some gaps presented in the specialized literature:

Research gap 1: There is no use of inverse droop controllers in the Optimal Power Flow of islanded grids with a low r/x ratio, which has been demonstrated to be more efficient for grids with such characteristics as demonstrated in (Garcès and Gil-Gonzàlez, 2021). Although its inclusion does not modify the problem's difficulty, it would be appropriate to analyze by considering its incorporation into the OPF.

Research gap 2: Existing articles neglect the effect of frequency on the optimal power flow for stand-alone microgrids. Furthermore, they do not specify the reason for not including it in the Y_{bus} variation. For this reason, it is necessary to analyze its inclusion and the possible changes by including it.

Research gap 3: Most of the articles reviewed in state-of-the-art are based on the branch flow equations (BFM), which are preferred over bus injection formulation (BIM). However, they are only applicable to radial grids; furthermore, there is almost no evaluation of the proposals in benchmarks with meshed grids.

In this aspect, convex optimization emerges as one of the effective techniques applied to Active Distribution Networks thanks to their properties such as global optimum, uniqueness of the solution and fast convergence (Low, 2014). For these reasons, two optimization problems are developed in the present work taking into account the research gaps described above in order to effectuate the optimal operation of single phase and three-phase distribution networks.

1.3 Objectives

1.3.1 General objective

To develop an optimization model strategy for the optimal operation of ADNs in islanded state, considering the frequency effect and the generation variation (such as deficit or surplus).

Specific objectives

- To formulate an optimization model that considers the elements associated with the operation of ADNs.
- To identify if the inverse droop control is suitable for carrying operative studies related to grid with low r/x ratio (such as ADNs or microgrids)
- To formulate several optimization methodologies that allow to handle the operation of islanded ADNs in order to determine which one has better performance
- To recognize the influence of deficit and surplus of generation in the Optimal Power Flow in order to measure the frequency and voltage variation employing dynamic simulations.
- To validate the proposal into several benchmarks.

1.4 Contributions

The major contributions of this master thesis are:

- To include the inverse droop into the OPF to control the operation of the active distribution networks during grid islanded mode.
- A unified, generic scheme for the optimal power flow during grid islanded and grid connected mode.
- An analysis regarding the effects of including the frequency into the Y_{bus} in grids with High r/x ratio.

1.4.1 List of Publications

Journals

- **IFAC-Papers online**: Conference with publication in Science-Direct with Q3 index. The problem of the islanded operation was addressed employing sequential approximation (Sepulveda et al., 2022b).

- **TecnoLogicas**: A Stability Analysis of the Voltage Source Converter has been presented in a journal with Q3 index, (Sepúlveda García and Garcés, 2022). This paper is not directly related to the OPF. However, it was the first attempt to understand the effect of the droop control in microgrids.

- A Unified Framework for the Optimal Operation of Active Distribution Networks. *Under revision in* - Electrical Engineering (Springer) Q2. This paper presents the proposed methodology in balanced ADN.

- Optimal Operation of Three-Phase islanded Active Distribution Networks. *ongoing*. This paper extends the methodology to three-phase unbalanced ADNs.

Conferences

- **11th IFAC Symposium on Control of Power and Energy Systems, CPES 2022, Moscow, Russia**. Conference organized by the international federation of automatic control (IFAC) in Moscow, Russia. The presentation was online due to the limitations given by the Russia-Ukrania war. The paper and the presentation are available in (Sepulveda et al., 2022b).

- **IEEE-Andescon 2022, Barranquilla, Colombia** This paper was a modification to the work presented by (Ramirez et al., 2021). Here, we considered the delta loads, since in the specialized literature they are usually neglected for the three-phase case. The paper presented in Barranquilla is available in IEEExplorer in (Sepúlveda et al., 2022).

- **IEEE General-Meeeting 2022, Denver, Colorado**: An optimization model based in the second order cone approximation has been presented to operate the grids during islanded mode. Available in IEEExplorer in (Sepulveda et al., 2022a).

Other works

The following works were developed during the master program, although they are not part of the present thesis:

- Power Flow Solution in Bipolar DC Networks Considering Neutral Wire and Unbalanced Loads: A Hyperbolic Approximation - Algorithms MDPI Q2 (Sepúlveda-García et al., 2022).

- Second Order cone Branch Flow model Approximation for the Optimal Power Flow in Bipolar Grids *under revision* -International Journal of Electrical Power & Energy Systems, Q1.

- Sequential Quadratic Approximation for the OPF Problem in Bipolar Grids with Unbalanced Constant Power Terminals *under revision* - Results in Engineering, Q1.

1.5 Document organization

The rest of the document is organized as follows: Chapter 2 discusses the hierarchical control in active distribution networks and microgrids. The primary and secondary control are briefly discussed, whereas we focus on the tertiary control (since it is the focus area of this document). Chapter 3 introduces the optimal control in active distribution networks, a generic optimization model which includes grid connected and grid islanded is presented, in this chapter it is presented the model of the grid, and models of several components such as wind, solar photovoltaic, batteries, among others. In chapter 4 we discuss the convex approximations for generic optimal power flow in active distribution networks. In chapter 5, some simulations are performed in several benchmarks, a brief discussion about the results is presented; finally, in chapter 6 the conclusions and future works are presented. A schematic representation of the document organization is presented in Figure 1.1.

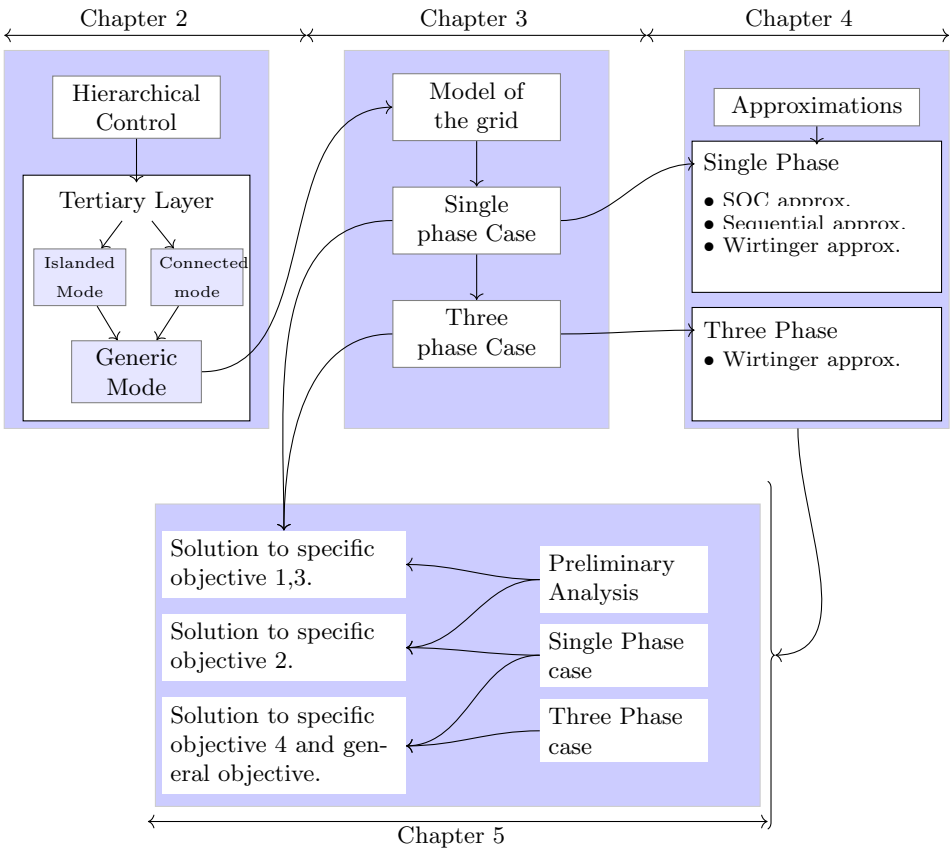

Figure 1.1: Document organization

Chapter 2

Hierarchical Control in Active Distribution Networks

Active distribution networks are electrical systems operating in low or medium voltage. As discussed in Chapter 1, they correspond to an evolution of the conventional distribution grids with high penetration of communication technologies, automatization of the grid, and the inclusion of distributed generators (DGs), battery energy storage systems (BESS), and electric vehicles. Figure 2.1 shows a schematic representation of this type of networks.

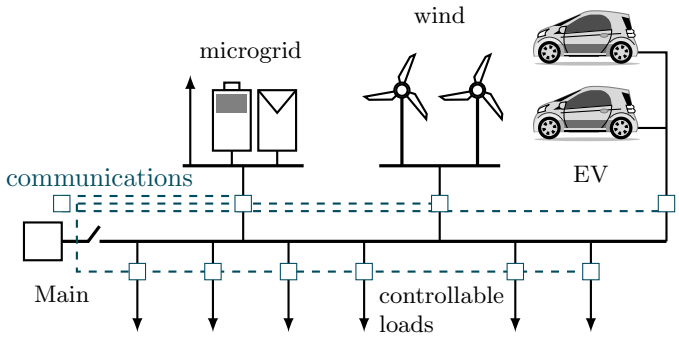

Figure 2.1: Schematic representation of an active distribution network (Figure taken from (Sepulveda et al., 2022b)).

Besides the elements mentioned above, ADNs could include several mi-

crogrids, which are more significant in capacity and robustness. This aggregation of microgrids in an active distribution network leads to confusion between each other since they have similar features. Both a microgrid and an ADN may have a low r/x ratio and include technologies such as distributed generation and controllable loads (Wu and Sansavini, 2021); in this document, both terms are used interchangeably since the proposed operation model is applicable for both. Moreover, ADNs can operate in grid-connected mode, where the primary grid imposes the voltage reference and the frequency, or in islanded mode, where the voltage and the frequency need to be coordinated between the DGs that contain some droop control scheme (Shahgholian, 2021). The main difference is the size of the network. Notice that an algorithm designed for ADN may be used for microgrids but not the opposite.

In order to obtain benefits such as lower power loss, enhanced resiliency, reliability, and improved efficiency, supervisory control must be executed in real-time. This control is part of the hierarchical structure usually named primary, secondary, and tertiary control (Planas et al., 2013). The classical control of power systems inspires this hierarchical control. The primary layer stabilizes the grid's frequency and voltage; the secondary layer balances active and reactive power; the tertiary layer is in charge of the optimal dispatch of generation and storage units (Yamashita et al., 2020). Notice that some authors decouple the primary control into primary and zero control, considering levels instead of three. A schematic representation of the hierarchical control is presented in Figure 2.2

The layers of the control are executed in different time windows. The fastest control corresponds to the zero level and the corresponding first layer. The secondary control is executed in order of seconds, whereas the tertiary is executed during steady state operation, which is in the order of minutes. The main characteristics of each layer are described below.

2.1 Level-zero and primary control

2.1.1 Level-zero control

Most distributed energy resources incorporate a voltage source converter (VSC) to integrate the generator (or the battery) into the three-phase grid. Level zero control acts directly on the converter; hence, it has the fastest dynamic. This control stabilizes voltage and frequency, performs island-

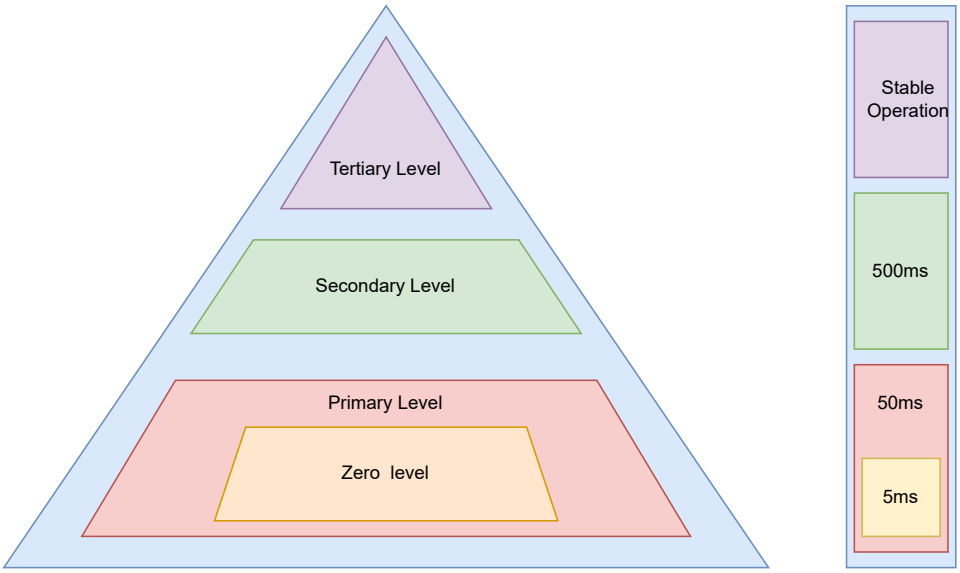

Figure 2.2: Hierarchical control of active distribution networks, including typical time window for each control

ing detection, and executes power-sharing, among other actions (Yamashita et al., 2020; García-Ceballos et al., 2021). There are many types of level-zero control in the scientific literature. They could be classified into three categories, depending on their purposes. these categories are given in Table 2.1.

Table 2.1: Type of control for layer-zero according to converters' functionality (Rocabert et al., 2012)

Type of converter	Functionality	Control
Grid Forming	Voltage and frequency control	V-f droop based control
Grid Following	Power dispatch	Vector oriented control
Grid supporting	Reactive power support	AC-V control

Level zero control varies according to the type of converter (Ansari et al., 2021). It could control active or reactive power, as in the grid-following converters, or voltage and frequency, as in the grid-forming converter. Ancillary services can be included as in the grid-supporting converters (Rocabert et al., 2012). An ADN could contain at least a significant part of its DGs operat-

ing as grid-following to alleviate the power flow through the lines. It may also contain grid-forming converters to control the voltage and frequency during the grid-islanded mode. Some authors consider that this control is independent of the primary control, since the primary control involves the mandatory use of $v \sim \omega$ droop schemes in order to effectuate the control of the voltage and frequency.

Figure 2.3 shows a schematic representation of a conventional grid- following converter that integrates renewable energy resources. It consists of a phase-locked loop (PLL) that synchronizes with the primary grid; an inner loop that controls the output current; and an outer loop that controls either the DC voltage and the reactive power or the active and reactive power. In both cases, the converter can be represented as a PQ node for steady-state analysis.

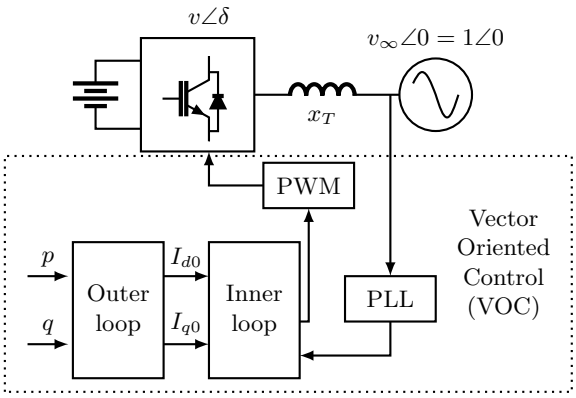

Figure 2.3: Example of grid following converters and its internal control (Vector Oriented Control, VOC).

Grid-following converters may not participate in the primary, secondary, or tertiary control since they cannot effectuate control over v and ω. Instead, they are PQ nodes in the stationary state. Usually, $q = 0$ to maintain a unity power factor. On the other hand, grid-forming converters participate directly in the primary, secondary, and tertiary layers of control to maintain v and ω between a stable range of operations. The following section describes these aspects in more detail.

2.1.2 Primary control

The primary control is mainly in charge of stabilizing the grid after a disturbance. This control incorporates droop schemes intended to secure an equilibrium point of operation while maintaining voltage and frequency among their normal range (Bravo-López et al., 2021). As described above, the primary control is the fastest layer after the zero level. It could include several ancillary services (mostly related to power quality issues).

The classical control is $p \sim \omega$ and $q \sim v$ scheme, which emulates the inertial behavior of a synchronous machine, compensating the mismatch between generation and demand (Yamashita et al., 2020). This droop scheme controls the frequency (voltage) with the active power (reactive power). This droop scheme has been demonstrated to be accurate for grids with low r/x ratio, for example, the power systems. However, active distribution networks and microgrids are characterized for presenting a high r/x ratio since the lines are short and operate in low voltage. For this reason, several studies have been carried out, demonstrating that for low voltage grids, it is preferable to employ the *inverse-droop* control (Garcès and Gil-Gonzàlez, 2021) (see Figure 2.4 for a schematic representation of a inverse droop control).

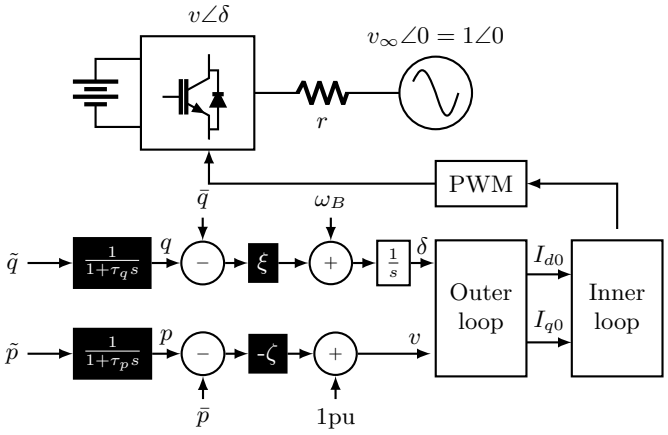

Figure 2.4: Schematic representation of inverse grid-forming converters

The inverse droop controls the voltage and frequency using active and reactive power. It presents a different relation between those variables, as observed in Figure 2.5. Conventional droop is used in system where $x >> r$, while inverse droop is used in highly resistive systems.

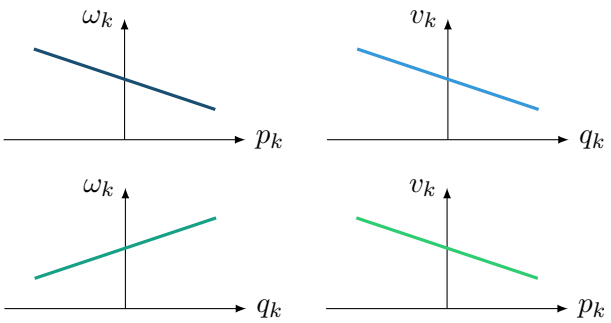

Figure 2.5: Primary control: conventional droop controls (above) and inverse droop controls (below)

The conventional droop control is mathematically described in steady state as presented below:

$$\omega_k - w_0 = -\zeta_k(p_k^g - \bar{p}_k) \tag{2.1}$$
$$\|\mathbf{v_k}\| - \bar{u}_k = -\xi_k(q_k^g - \bar{q}_k) \tag{2.2}$$

while the inverse droop control is described as follows:

$$\omega_k - w_0 = \xi_k(q_k^g - \bar{q}_k) \tag{2.3}$$
$$\|\mathbf{v_k}\| - \bar{u}_k = -\zeta_k(p_k^g - \bar{p}_k) \tag{2.4}$$

where ω_k, v_k, p_k^g and q_k^g represents the frequency, voltage and active power and reactive power respectively, for each node that contains a power converter; ω_k, v_k, p_k^g; ω_0, $\bar{u}_k$, $\bar{p}_k$ and $\bar{q}_k$ correspond to their nominal values; ζ_k, ξ_k are the droop constants. From the inverse droop controller, it is possible to observe that the second equation is non-linear and non-convex. Therefore, it introduces a source of complexity in the optimization model. In this work, we consider that most distributed generators contains a zero layer control that allows them to act as grid-following converters, delivering all its available energy during grid connected mode. Besides, some generators contain droop schemes that allow them to implement the primary control in order to maintain stable the frequency and voltage. Both, direct and inverse droop are considered.

2.2 Secondary control

Secondary control shares some characteristics of primary and tertiary controls. It is an algorithm that carries variables such as frequency and voltage to its nominal value (or the optimal point given by the tertiary control) (Dragičević, 2018). This layer needs to be well-designed since microgrids and ADNs may have low inertia; hence, they are more susceptible to voltage and frequency variations. In each step, it must be stabilized, and characteristics of the tertiary control since an optimization model is required to reach the optimal (or nominal) value. A visual representation of the three layers of control is depicted in Figure 2.6, where it is possible to observe the nature of the each layers.

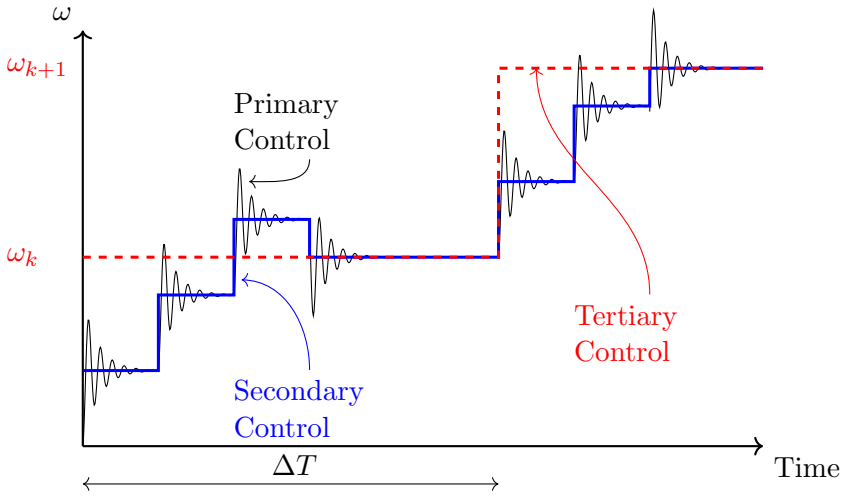

Figure 2.6: Dynamic behavior for each control layer (Adapted from (Rios and Garces, 2022))

The secondary layer could be centralized or distributed. Communication technologies are required in both cases. The former is easy to implement in real-life situations and allows more efficient algorithms. However, the latter may lead to more robust and secure communication architectures (Khayat et al., 2020). The dynamic response due to this layer is fast enough (compared to the tertiary layer) and could be neglected in the analysis. As mentioned, the purpose of the second layer is to adjust the generators to the optimal points obtained in the tertiary layer.

2.3 Tertiary control

The tertiary control corresponds to the upper layer in the hierarchical control. Some authors contemplate an execution time of about 5 to 15 minutes (in a daily operation horizon). For this reason, it is considered only to be effectuated during stable state operation (depreciating the effects of the first two layers) (Abdi et al., 2017). As could be noticed, the first two layers mainly focused on the network's dynamic response (i.e., the grid's technical features). However, distribution operators mainly intend to obtain profit from the operation of the distribution grid. For this reason, the tertiary layer is in charge of effectuating the optimal functioning of the grid, generally regarding some economic aspects, but technical as well (such as the reduction of the power losses and technical constraints) (Risi et al., 2022). The tertiary layer is usually an optimization model of the form Garcés Ruiz (2020):

$$\begin{aligned} &\min \quad f(x) \\ &s.t. \\ &h(x) \leq 0 \\ &g(x) = 0 \end{aligned} \tag{2.5}$$

where $f(x)$ corresponds to the objective function (usually operation cost or power loss); $h(x)$ corresponds to the set of inequality constraints representing technical limits such as the thermal capacity of distribution lines, voltage deviation, maximum power provided by a distributed generator, among others; $g(x)$ corresponds to the set of equality constraints that represent the power balance (i.e., the power flow equations). The optimal power flow problem is mainly a non-linear programming model. It is non-convex since it contains non-affine equality contains (Molzahn and Hiskens, 2019). There are two main variants regarding the tertiary control of active distribution networks:

Centralized control : Requires low investment since a central module receives all the signals concerning the state of distributed generators and loads, performs the optimal power flow and send the optimal dispatch to the power converter control associated with distributed generators. The main problem of this architecture, is because it is more vulnerable to cyber-attacks, or to total failures if the central module fails (Saleh et al., 2019).

Distributed control : Requires higher investments, a distributed consensus is performed between all the distributed generators in order to operate (together) optimally the grid, it is more reliable since it could operate even if a given communication line (or DG) goes out of operation (known as single-point failure) (Engelmann et al., 2019, 2017).

In the present work, we focus on the centralized control since a distribution operator could receive, supervise and manipulate in real-time all the system's variables from a single point (substation). Notice that the dynamics of microgrids may change a lot and hence, the frequency may be not arrived to stationary state when the tertiary control acts. Therefore, it is important to include the effect of the frequency in the tertiary control.

2.4 Operation modes

An active distribution network may operate in grid-connected or islanded mode. The hierarchical control can act in both modes, but the optimization model requires to be adapted accordingly. These operating modes are presented in Figure 2.7 and described below.

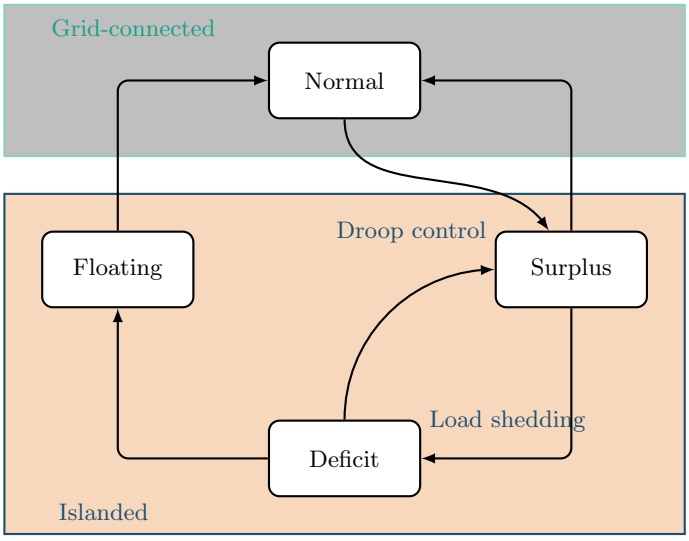

Figure 2.7: Operation modes of active distribution networks

2.4.1 Grid-connected operation

During grid-connected operation, the tertiary layer is mainly intended to effectuate the optimal power flow regarding economical aspects and technical constraints. The slack node imposes voltage reference and frequency, and it is able to compensate the surplus and deficit of generation of the distributed generators. For this reason, the distributed generators could deliver all its available power (grid following). Nowadays' studies related to grid connected mode are mainly focuses on answer two questions: How many electric vehicles (EVs) are able to support the active distribution network? (Zhu et al., 2022) How much penetration of distributed generator is able to support the active distribution network? (Hou et al., 2022) Both questions are part of what is known as hosting capacity.

2.4.2 Grid islanded operation

In grid-islanded mode, the tertiary layer must consider technical aspects such as voltage regulation and frequency. For this reason, some distributed generators equipped with droop schemes stop delivering all their available power and start regulating the frequency and voltage (Guerrero et al., 2011). Hence, they can change from grid-following to grid-forming.

It is important to remark that, during grid islanded operation, the primary and secondary layers stabilize the grid during the disconnection from the primary grid, load, generation, and other dynamics changes. We assume these layers achieve a stationary state after the events mentioned above, even if the final frequency differs from the nominal. Since these effects are faster than the tertiary layer, they are not considered in the present document. This proposal assumes that the first two layers operate correctly, and the sole purpose of the tertiary layer is to set the optimal operation values while ensuring a safe range of operation of the variables.

In grid-islanded mode, three different types of operation could happen. The first one is the **surplus of generation**, where the available power of the distributed generators is greater than the load in a given time. In this case, an economic dispatch regarding the technical constraints related to voltage and frequency regulation is effectuated. During **deficit of generation**, the distributed generators cannot feed all the loads. For this reason, some load shedding is performed to maintain the grid's stability. We call a third operation mode as **floating mode**, in which there is the presence of a slack

node (thus, voltage reference and the frequency are imposed by the primary grid). However, the main grid cannot provide or receive active or reactive power (i.e., the power injected from the slack node is equal to zero always); some authors have addressed this operation mode as (Ramirez et al., 2021). Eventough it needs to be clarified its applications. In the present work, we do not analyze this operation mode, since we consider that generation's deficit (surplus) is more general.

Finally, there are two transitive modes between GC and GI: re-connection and disconnection. The task of re-connection and stabilizing the grid after disconnection is effectuated by the secondary and primary layers, and hence is depreciated in this document.

Chapter 3

Optimal Operation in Active Distribution Networks

3.1 Model of the grid

An active distribution network, such as the one shown in Figure 2.1 can be mathematically represented by an oriented graph $\mathcal{F} = \{\mathcal{N}, \mathcal{E}\}$, where $\mathcal{N} = \{1, 2, 3, .., n\}$ is the set of nodes (with n being the number of nodes of the grid); phases are represented by the set $\mathcal{P} = \{a, b, c\}$; $\mathcal{E} = \{\mathcal{N} \times \mathcal{N}\}$ is the set of branches of the grid[1]. Furthermore, $\mathcal{G} \in \{\mathcal{N}\}$ is the set of generators (with $\mathcal{B} \subset \mathcal{N}$ being the set of Battery Energy Storage Systems, BESS), $\mathcal{L} \in \{\mathcal{N}\}$ the set of loads and $\mathcal{T}$ the set of times (Lavaei and Low, 2012). A simplified representation of a generic node k and its neighboring nodes is presented in Figure 3.1.

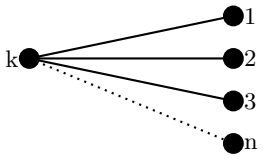

Figure 3.1: Nodal (and equivalent) representation of a grid

From the first Kirchhoff law's it is possible to obtain the following ex-

[1] in this context $\times$ represents the cartesian product

pression on the complex domain:

$$\mathbf{i_k} = \sum_{m \in \Omega_k} \mathbf{i_{km}} \tag{3.1}$$

where $\mathbf{i_k}$ is the current injection in the node $k \in \mathcal{N}$, and $\mathbf{i_{km}}$ is the current flow from node k to its neighbors Ω_k; bold letters represent complex variables (or constants). On the other hand, nodal and branch currents are given by the following two equations:

$$\mathbf{i_k} = \left(\frac{\mathbf{s_k}}{\mathbf{v_k}}\right)^* \tag{3.2}$$

$$\mathbf{i_{km}} = (\mathbf{v_k} - \mathbf{v_m})\mathbf{y_{km}} \tag{3.3}$$

Where (3.2) is the relation between power, current, and voltage; in this equation, the apparent power is represented by $\mathbf{s_k} = \mathbf{s_k^g} - \mathbf{s_k^d}$ that comprises the power injection $\mathbf{s^g}$, and the power demanded $\mathbf{s^d}$. The voltage at node k is represented by $\mathbf{v_k}$ where the operator $\mathbf{x}^*$ is the conjugate of $\mathbf{x}$. The second equation corresponds to Ohm's law, and $\mathbf{y_{km}}$ represents the admittance between nodes k and m. It is possible to obtain a generic equation for single phase representation that relates the power injection and power flow through the lines that connect k with its neighboring nodes by replacing the two equations described above into (3.1):

$$\mathbf{s_k^*} = (\mathbf{s_k^g} - \mathbf{s_k^d})^* = \mathbf{v_k^*} \sum_{m \in \Omega_k} \mathbf{v_m y_{km}} \tag{3.4}$$

which is a representation for a given node k. It could be generalized into a matrix form by stacking the voltage and powers as follows[2]:

$$\mathbf{V} = \begin{pmatrix} \mathbf{v_1} \\ \mathbf{v_2} \\ \vdots \\ \mathbf{v_{n-1}} \\ \mathbf{v_n} \end{pmatrix}, \ \mathbf{S} = \begin{pmatrix} \mathbf{s_1} \\ \mathbf{s_2} \\ \vdots \\ \mathbf{s_{n-1}} \\ \mathbf{s_n} \end{pmatrix} \tag{3.5}$$

Taking into account the vectorized form of v and s, (3.4) conduces to:

$$(\mathbf{S^g} - \mathbf{S^d})^* = \mathbf{V}^* \circ \mathbf{Y}_{\text{bus}}\mathbf{V} \tag{3.6}$$

[2]Capital letters represent vectorized variables

where $\circ$ corresponds to the Hadamard product, which effectuates the element-wise multiplication between matrices or vectors (Axler, 2015). Equation (3.6) is known as the standard power flow formulation; it is a non-linear and non-convex equation due to its bilinear form. The admittance matrix, $\mathbf{Y}_{\text{bus}}$, indicates the physical connection between nodes. It is constructed taking into account the branch-to-node incidence matrix A. The latter indicates the physical connections between nodes and branches of the active distribution network. The equation for calculating $\mathbf{Y_{bus}}$ is given below (Stevenson, 1982):

$$\mathbf{Y}_{\text{bus}} = A^{\top}\mathbf{Y_p}A \tag{3.7}$$

Where $\mathbf{Y_p}$ represents the primitive admittance connection between nodes. Some authors decouple Equation (3.6) into two equations. The first is linear and allows the calculation of the power injected by the slack node, and the second, non-linear, allows the calculation of the voltage in the grid nodes. During this document, we do not make that distinction since the slack node concept is only valid during grid-connected mode; however, during the islanded mode, there is no presence of a slack node.

Calculating Y_{bus} for three-phase systems remain the same as (3.7), the main difference lies in the incidence matrix which is calculated as follows:

$$\mathbf{Y}_{\text{bus},\mathbf{3}\phi} = (I_3 \otimes A^{\top})\mathbf{Y}_{\mathbf{p},\mathbf{3}\phi}(I_3 \otimes A) \tag{3.8}$$

where I_3 is the identity matrix with size 3×3 and $\otimes$ is known as the Kronecker product; $Y_{p,3\phi}$ is the 3-phase primitive matrix that represent the physical (and mutual) admittance connections between nodes and phases (Kersting, 2017). The matrix expression for calculating the power balance for the three-phase changes to the form:

$$\mathbf{S^g} - \mathbf{S^d} = \text{diag}(\mathbf{V})\mathbf{Y}^{*}_{\text{bus},\mathbf{3}\phi}\mathbf{V}^{*} \tag{3.9}$$

where $\text{diag}(x)$ converts the vector x into a diagonal matrix with zeros outside the main diagonal, in both cases the power balance is non-linear and non-convex. Generally, an equality constraint needs to be affine in order to be convex, and for both cases it is a quadratic constraint; hence, it is still non-convex (Low, 2014).

For the three-phase case, it is important to denote that the voltage vectors (and power injections) are stacked following the order nodes-phases as

follows:

$$\mathbf{V} = \begin{pmatrix} \mathbf{v_{1,a}} \\ \mathbf{v_{1,b}} \\ \mathbf{v_{1,c}} \\ \vdots \\ \mathbf{v_{n,a}} \\ \mathbf{v_{n,b}} \\ \mathbf{v_{n,c}} \end{pmatrix}, \ \mathbf{S} = \begin{pmatrix} \mathbf{s_{1,a}} \\ \mathbf{s_{1,b}} \\ \mathbf{s_{1,c}} \\ \vdots \\ \mathbf{s_{n,a}} \\ \mathbf{s_{n,b}} \\ \mathbf{s_{n,c}} \end{pmatrix} \tag{3.10}$$

The analysis remains the same, just in this case there are three slack nodes (for the grid connected model) and the Y_{bus} is three-phase.

3.2 Model of distributed energy resources

In this section, we present the generic model of the DGs. Furthermore, we present the model of the solar panel and wind turbine. For this study we use satellite data collected from the web page (NASA, 2023), that allows to observe variables such as irradiance, temperature, and wind speed.

3.2.1 Distributed generators

We represent distributed generators as constant power sources that are able to deliver all its available power during grid-connected mode. They are able to maintain frequency and voltage among their normal range of operation during grid-islanded mode. These type of distributed resources are known as grid forming converters. Some of the technical constraints that a given distributed resource at node k requires following during islanded operation mode are given below:

$$\|\mathbf{s_k^g}\| \leq s_k^{\max} \tag{3.11}$$
$$p_k^{\min} \leq p_k^g \leq p_k^{\max} \tag{3.12}$$
$$q_k^{\min} \leq q_k^g \leq q_k^{\max} \tag{3.13}$$
$$\omega_k - 1 = \xi_k(q_k^g - q_k^{\max}) \tag{3.14}$$
$$\|\mathbf{v_k}\| - \bar{u}_k = -\zeta_k(p_k^g - p_k^{\max}) \tag{3.15}$$

Equation (3.11) represents the maximum apparent power that a distributed generator could deliver to the main grid; Equations (3.12)-(3.13)

represent the boundaries (maximum/minimum), active and reactive power that a distributed resource can inject to the grid. Some authors consider these three equations redundant, since with equation (3.11) and (3.12) could be obtained (3.13) (and viceversa, with Equations (3.12) and (3.13) could be obtained Equations(3.11)). The respective operation costs of DGs are assumed in the specialized literature to follow a quadratic function, as given below (Huang et al., 2022b):

$$p_{\text{cost}} = c_2(p^g)^2 + c_1 p^g + c_0 \tag{3.16}$$

where c_2, c_1 and c_0 represents the constants of the quadratic cost function. Linear cost are also possible in the model.

3.2.2 Model of solar panels

The model of the solar panel adopted here is the classical model described in (Wang et al., 2018). The active power of this model is mainly affected by solar radiation and the temperature, which can be expressed as follows:

$$P_{pv} = P_{STC}\frac{G_c}{G_{STC}}(1 + k(T_c - T_{STC})) \tag{3.17}$$

Where P_{pv} is the output power of the photovoltaic units; T_c is the temperature on the surface of the PV units; G_c is the radiance at the surface of the PV units; and k, is the power temperature coefficient. G_{TSC} is the standard radiance (1000 W/m^2) and T_{TSC} is the standard temperature which is 25 °C, and P_{STC} is the rated power output of solar PVs.

3.2.3 Model of wind turbines

The model for wind generators is described in reference (Masters, 2004). It relates the output power of a wind turbine vs. wind speed via a piecewise function as given below:

$$P(v) = \begin{cases} p_r(v - v_{ci})/(v_r - v_{ci}) & v_{ci} \leq v \leq v_r \\ p_r & v_r \leq v \leq v_{co} \\ 0 & v < v_{ci} \quad \text{or} \quad v > v_{co} \end{cases} \tag{3.18}$$

Where P is the output power of the wind turbine, v is the current wind speed of the Wind turbine. v_{ci} is the cut-in speed, v_{co} the cut-out wind

speed, v_r the nominal wind speed and p_r the nominal power of the wind units.

3.2.4 Model of energy storage systems

Battery energy storage systems are a vital element for Active Distribution Networks. For normal operation, the batteries are charged during low demand hours and discharged during peak hours since it alleviates the power flow; furthermore, BESS allows integrating DGs with a variable (stochastic) nature, such as the Photovoltaic units and Wind turbines, in order to compensate such intermittence.

In the specialized literature, there are predominantly two models for the BESS while addressing the Optimal operation or planning. The first one is proposed in (Gil-González et al., 2019), has a linear nature as observed in equation (3.19), Where $e_{k,t}$ represents the State Of Charge of the Battery in a time t, Φ the efficiency of the Battery, ΔT represents the time window of the operation (ΔT is assumed as 1 hour in this work) and $p_{k,t}$ the power injection of the BESS.

$$e_{k,t} = e_{k,t-1} - \Phi p_{k,t} \Delta T \tag{3.19}$$

This is a simplified model that does not consider the internal power losses of the battery, and could deliver or receive energy from the main grid at the same time. The second model of BESS could be found in (Macedo et al., 2015), it is a mixed integer linear equation that separates the charging and discharging power ($p^c_{j,t}$ and $p^{dc}_{j,t}$ respectively) with their corresponding efficiencies (η^c and η^{dc} respectively).

$$e_{j,t} = e_{j,t-1} + \eta^c p^c_{j,t} \Delta T - \frac{1}{\eta^{dc}} p^{dc}_{j,t} \Delta T - \beta e_{j,t-1} \tag{3.20}$$

This equation also considers the internal losses by introducing a self discharge rate of the battery β. This is a more complex model of the BESS due to the introduction of binary variables (x_t) associated with technical constrains in order to completely separate the charging and discharging power

as listened below:

$$p^{c}_{\min} x_t \leq p^{c}_{j,t} \leq p^{c}_{\max} x_t \tag{3.21}$$

$$p^{dc}_{\min}(1 - x_t) \leq p^{dc}_{j,t} \leq p^{dc}_{\max}(1 - x_t) \tag{3.22}$$

$$e_{\min} \leq e_{j,t} \leq e_{\max} \tag{3.23}$$

$$\tag{3.24}$$

where the first equation represent the maximum power charge that the battery could afford in a given time, the second equation represents the maximum power discharge that a given battery could afford, and the final equation represent the maximum capacity of the battery. Additionally, other two equations that relates the initial and final State of charge are employed. In a given NLP problem, the introduction of BESS with this formulation transforms it into a mixed-integer non-linear programming model.

3.3 Technical constraints

Other technical constraints are related to the maximum capacity of PV and wind units, for example:

$$p^{\min}_{k} \leq p^{wind}_{k} \leq p^{\max}_{k} \tag{3.25}$$

$$0 \leq p^{pv}_{k} \leq p^{\max}_{k} \tag{3.26}$$

Maximum deviation of the voltage in all the nodes:

$$v^{\min} \leq \|\mathbf{v}\| \leq v^{\max} \tag{3.27}$$

Maximum deviation of the frequency while operating in grid-islanded mode:

$$\omega^{\min} \leq \omega \leq \omega^{\max} \tag{3.28}$$

Or maximum current flow through the lines:

$$\|(\mathbf{v_k} - \mathbf{v_y})\mathbf{y_{km}}\| \leq i^{\max} \tag{3.29}$$

These constrains are included into the model in order to obtain a generalized optimization problem. This problem may be balanced or unbalanced, as shown in the next sections.

3.4 Balanced case (single-phase equivalent)

In this section, we present the generic Optimal Power Flow formulation for both, grid-islanded and grid-conected modes of active distribution networks. The model is mathematically described by equations (3.30) - (3.49) and is a MINLP problem due to the presence of binary variables.

Obj. function:

$$\min \sum_{\substack{t=1\\ t\in\mathcal{T}}} c^s p_t^s(1-\alpha_t^s) + \sum_{\substack{t=1\\ t\in\mathcal{T}}}\sum_{\substack{k=1\\ k\in\mathcal{G}}}^{n} c_{k,t}^g p_{k,t}^g + \sum_{\substack{t=1\\ t\in\mathcal{T}}}\sum_{\substack{k=1\\ k\in\mathcal{L}}}^{n} c_{k,t}^d p_{k,t}^d(1-\alpha_{k,t}^d) \tag{3.30}$$

Subject to:

$$\begin{aligned} p_t^s + p_{k,t}^g + p_{k,t}^c - p_{k,t}^{dc} + p_{k,t}^{sol} - p_{k,t}^d\alpha_{k,t} + \\ j(q_{k,t}^d\alpha_{k,t}^d - q_{k,t}^{cap} - q_{k,t}^g - q_t^s) = \sum_{m\in\mathcal{N}} \mathbf{y}_{km}\mathbf{v}_{k,t}^*\mathbf{v}_{m,t} \quad \forall k\in\mathcal{N}, \quad \forall t\in\mathcal{T} \end{aligned} \tag{3.31}$$

$$\|\mathbf{v_{k,t}} - 1\| \leq \delta \quad \forall k\in\mathcal{N}, \quad \forall t\in\mathcal{T} \tag{3.32}$$

$$p_k^{\min} \leq p_{k,t}^g \leq p_k^{\max} \quad \forall k,\in\mathcal{G}, \quad \forall t\in\mathcal{T} \tag{3.33}$$

$$q_k^{\min} \leq q_{k,t}^g \leq q_k^{\max} \quad \forall k\in\mathcal{G}, \quad \forall t\in\mathcal{T} \tag{3.34}$$

$$(1-\alpha_t^s)p_s^{\min} \leq p_t^s \leq p_s^{\max}(1-\alpha_t^s) \quad \forall t\in\mathcal{T} \tag{3.35}$$

$$(1-\alpha_t^s)q_s^{\min} \leq q_t^s \leq q_s^{\max}(1-\alpha_t^s) \quad \forall t\in\mathcal{T} \tag{3.36}$$

$$0 \leq pv_{k,t} \leq pv_{k,t}^{\max} \quad \forall k\in\mathcal{G}|\mathcal{G}=pv \quad \forall t\in\mathcal{T} \tag{3.37}$$

$$(x_{k,t})pb^{\min} \leq pb_{k,t}^c \leq pb^{\max}(x_{k,t}) \quad \forall k\in\mathcal{B}, \quad \forall t\in\mathcal{T} \tag{3.38}$$

$$(1-x_{k,t})pb^{\min} \leq pb_{k,t}^{dc} \leq pb^{\max}(1-x_{k,t}) \quad \forall k\in\mathcal{B}, \quad \forall t\in\mathcal{T} \tag{3.39}$$

$$e_k^{\min} \leq e_{k,t} \leq e_k^{\max} \quad \forall k\in\mathcal{B}, \quad \forall t\in\mathcal{T} \tag{3.40}$$

$$1-\Delta\omega \leq \omega_{CI,t} \leq 1+\Delta\omega \quad \forall t\in\mathcal{T} \tag{3.41}$$

$$\omega_{k,t} - \omega_0 = \xi_k(q_{k,t}^g - q_k^{\max}) \quad \forall k\in\mathcal{G}\wedge\alpha_t^s=1, \quad \forall t\in\mathcal{T} \tag{3.42}$$

$$\|\mathbf{v_k}\| - \bar{u}_k = -\zeta_k(p_{k,t}^g - p_k^{\max}) \quad \forall k\in\mathcal{G}\wedge\alpha_t^s=1, \quad \forall t\in\mathcal{T} \tag{3.43}$$

$$e^b_{k,t} = e^b_{k,t-1} - \eta^c pb^c_{k,t}\Delta T - \frac{1}{\eta^{dc}} pb^{dc}_{k,t}\Delta T \quad \forall k \in \mathcal{B}, \quad \forall t \in \mathcal{T} \tag{3.44}$$

$$e_{k,t=0} = e^{bf}_k \tag{3.45}$$

$$e_{k,t=24} = e^{bo}_k \tag{3.46}$$

$$\|(\mathbf{v_k} - \mathbf{v_y})\mathbf{y_{km}}\| \leq i^{\max} \quad \forall (km) \in \mathcal{E}, \quad \forall t \in \mathcal{T} \tag{3.47}$$

$$\omega_{CI,t} = \frac{\sum_{k\in\mathcal{N}} \xi_k^{-1}\omega_k}{\sum_{k\in\mathcal{N}} \xi_k^{-1}} \quad \forall k \in \mathcal{G} \wedge \alpha^s_t = 1, \quad \forall t \in \mathcal{T} \tag{3.48}$$

$$\alpha_s, \alpha_d, x_t \in \{0, 1\} \tag{3.49}$$

The objective function seeks to reduce the overall costs of operation. The first terms refer to the energy costs imported from the primary grid (Slack node), and α^s_t indicates whether the slack node is connected or not. The second term refers to the operation costs of DGs, where it is assumed $c_2 = c_0 = 0$ to transform the model into an equivalent MILP. The third term refers to the cost of disconnection of loads, where the binary variable α^d_k indicates the disconnection of the load associated with node k; it is assumed that the cost of disconnection is greater than the cost of importing energy from the primary grid and that these costs are higher than the cost of generation of DGs.

The set of constraints is described as follows: (3.31) represents the power balance in each node of the system (where the left side of (3.4) has been expanded into real and imaginary part), as could be deduced it is a BIM formulation, where p^s_t, $p^g_{k,t}$, $p^c_{k,t}$, pk, t^{dc}, pk, t^{sol} and $p^d_{k,t}$ in the left-hand side of the equation represents the active power injected by the slack node, Distributed generator, a charge of BESS, discharge of BESS, PV units and loads respectively. $q^d_{k,t}$, $q^{cap}_{k,t}$ and $q^g_{k,t}$ represents the reactive power injected by the loads, capacitor banks, DGs and slack node, while the right-hand side of the equation represents the power flow through the lines of the grid. (3.32) represents the maximum deviation allowed of the voltage, which is assumed to be 10% of its nominal value. (3.33) - (3.41) represent the maximum capacity of generation for each distributed resource (both active and reactive power). Slack node (active and reactive power), PV units (active power since it is assumed that PV units operate with unitary power factor), power charging of BESS, power discharging of BESS (notice the binary variable x_t allows to only activate one state of the BESS per time), maximum Energy of the BESS, and a maximum deviation of frequency respectively. (3.42)-(3.43) represents the inverse droop control equations of the DGs that control the frequency with the reactive power and the voltage with the active power

since, for a stable state, all converters reach the same frequency, the concept of frequency centroid expressed in equation (3.48) is employed in order to unify the frequency, this equation has been employed in studies related to the secondary control as (Rios and Garces, 2022) and studies related primary control as (Garces, 2020) demonstrating its applicability. (3.44) represents the state of charge of the BESS, and (3.45) - (3.46) its initial and final state of charge. Furthermore, (3.47) represents the maximum current that could flow in the grid lines.

3.5 Three-phase case

The three-phase case differentiates in several equations from the single-phase case. Firstly, the objective function includes all the phases of the network. Some of the equations that are part of the set of constraints are written in a matrix form for each node (except for the power flow presented in Equation (3.52) which is for all the grid) of the system, and other constraints are written for each node and phase of the system. For this, it is essential to take into account that:

$$\mathbf{V_{k,t}} = \begin{pmatrix} \mathbf{v_{k,t,a}} \\ \mathbf{v_{k,t,b}} \\ \mathbf{v_{k,t,c}} \end{pmatrix} \tag{3.50}$$

$$\mathbf{V^{nom}} = \begin{pmatrix} 1 \\ \mathbf{e^{-2j\pi/3}} \\ \mathbf{e^{2j\pi/3}} \end{pmatrix} \tag{3.51}$$

furthermore new variables are introduced, these are $P_{3\phi}$, $Q_{3\phi}$, $P^s_{3\phi}$, $Q^s_{3\phi}$, PV and $PB^c_{3\phi}$ and are only defined for all the nodes of the system (and not for the phases).

Obj. Function:

$$\min \sum_{f\in\mathcal{P}}\sum_{\substack{t=1\\ t\in\mathcal{T}}} c^s_f p^s_{f,t}(1-\alpha^s_{f,t}) + \sum_{f\in\mathcal{P}}\sum_{\substack{t=1\\ t\in\mathcal{T}}}\sum_{\substack{k=1\\ k\in\mathcal{G}}}^{n} c^g_{k,f,t} p^g_{k,f,t} + \sum_{f\in\mathcal{P}}\sum_{\substack{t=1\\ t\in\mathcal{P}}}\sum_{\substack{k=1\\ k\in\mathcal{L}}}^{n} c^d_{k,f,t} p^d_{k,f,t}(1-\alpha^d_{k,f,t})$$

Subject to:

$$\mathbf{S_t^g} - \mathbf{S_t}^d \circ \alpha_t = \text{diag}(\mathbf{V_t}) Y_{\text{bus}}^* \mathbf{V_t}^* \quad \forall t \in \mathcal{T} \tag{3.52}$$

$$\|\mathbf{V_{k,f,t}} - \mathbf{V_f^{nom}}\| \leq \delta \quad \forall k \in \mathcal{N}, \forall f \in \mathcal{P}, \forall t \in \mathcal{T} \tag{3.53}$$

$$P_{3\phi,k,t} = \sum_{f \in \mathcal{P}} p_{k,t,f} \quad \forall k \in \mathcal{G}, \forall t \in \mathcal{T} \tag{3.54}$$

$$Q_{3\phi,k,t} = \sum_{f \in \mathcal{P}} q_{k,t,f} \quad \forall k \in \mathcal{G}, \forall t \in \mathcal{T} \tag{3.55}$$

$$PV_{k,t} = \sum_{f \in \mathcal{P}} pv_{k,t,f} \quad \forall k \in \mathcal{G} | \mathcal{G} = pv, \forall t \in \mathcal{T} \tag{3.56}$$

$$PB_{k,t}^c = \sum_{f \in \mathcal{P}} (pb_{k,t,f}^c) \quad \forall k \in \mathcal{B}, \forall t \in \mathcal{T} \tag{3.57}$$

$$PB_{k,t}^{dc} = \sum_{f \in \mathcal{P}} (pb_{k,t,f}^{dc}) \quad \forall k \in \mathcal{B}, \forall t \in \mathcal{T} \tag{3.58}$$

$$P_k^{\min} \leq P_{3\phi,k,t} \leq P_k^{\max} \quad \forall t \in \mathcal{T} \tag{3.59}$$

$$Q_k^{\min} \leq Q_{3\phi,k,t} \leq Q_k^{\max} \quad \forall t \in \mathcal{T} \tag{3.60}$$

$$(1 - \alpha_t^s) P_s^{\min} \leq P_{3\phi,t}^s \leq P_s^{\max} (1 - \alpha_t^s) \quad \forall t \in \mathcal{T} \tag{3.61}$$

$$(1 - \alpha_t^s) Q_s^{\min} \leq Q_{3\phi,t}^s \leq Q_s^{\max} (1 - \alpha_t^s) \quad \forall t \in \mathcal{T} \tag{3.62}$$

$$0 \leq PV_{k,t} \leq PV_{k,t}^{\max} \quad \forall t \in \mathcal{T} \tag{3.63}$$

$$(x_t) PB^{\min} \leq PB_{k,t}^c \leq PB^{\max} (x_t) \forall t \in \mathcal{T} \tag{3.64}$$

$$(1 - x_t) PB^{\min} \leq PB_{k,t}^{dc} \leq PB^{\max} (1 - x_t) \quad \forall t \in \mathcal{T} \tag{3.65}$$

$$E_k^{\min} \leq E_{k,t} \leq E_k^{\max} \quad \forall k \in \mathcal{B}, \forall t \in \mathcal{T} \tag{3.66}$$

$$1 - \Delta\omega \leq \omega_{CI} \leq 1 + \Delta\omega \quad \forall t \in \mathcal{T} \tag{3.67}$$

$$\omega_{k,t} - \omega_0 = \xi_k (Q_{3\phi,k} - Q_k^{\max}) \quad \forall k \in \mathcal{G}, \forall t \in \mathcal{T}, \wedge \alpha_s = 1 \tag{3.68}$$

$$V_{k,t}^{mag} - 1 = -\zeta_k (P_{3\phi,k} - P_k^{\max}) \quad \forall k \in \mathcal{G}, \forall t \in \mathcal{T}, \wedge \alpha_s = 1 \tag{3.69}$$

$$E_{k,t}^b = E_{k,t-1}^b - \eta^c PB_{k,t}^c \Delta T - \frac{1}{\eta^{dc}} PB_{k,t}^{dc} \Delta T \quad \forall k \in \mathcal{B}, \forall t \in \mathcal{T} \tag{3.70}$$

$$E_{k,t=0} = E_k^{bf} \tag{3.71}$$

$$E_{k,t=24} = E_k^{bo} \tag{3.72}$$

$$\omega_{CI} = \frac{\sum_{k \in \mathcal{G}} \xi_k^{-1} \omega_k}{\sum_{k \in \mathcal{G}} \xi_k^{-1}} \quad \forall k \in \mathcal{G}, \forall t \in \mathcal{T}, \wedge \alpha_s = 1 \tag{3.73}$$

$$V_k^{mag} = \|\mathbf{V_{k,a}}\| = \|\mathbf{V_{k,b}}\| = \|\mathbf{V_{k,c}}\| \quad \forall k \in \mathcal{G}, \forall t \in \mathcal{T} \tag{3.74}$$

$$\begin{aligned} \mathbf{s_{k,f,t}^g} = p_{k,t,f}^s + p_{k,t,f}^g + p_{k,t,f}^c - p_{k,t,f}^{dc} + p_{k,t,f}^{sol} \\ + j(-q_{k,t,f}^{cap} - q_{k,t,f}^g - q_{k,t,f}^s) \end{aligned} \tag{3.75}$$

$$\alpha_s, \alpha_d, x_t \in \{0, 1\} \tag{3.76}$$

It could be observed that, in general, all constraints remain with the same form or include a new subscript related to the phases of the system; naturally, it is essential to mention that the droops are now controlled concerning the sum of the three-phase (or the number of phases of the DG) active and reactive power of the generator; furthermore, the magnitude of the voltage (while considering GI operation) is equal for all the phases of the DG (or the number of phases of the DG that are delivering active power and contain droop control scheme). Moreover, the equation of the State Of the charge of BESS (see Equation (3.70)) is effectuated with the Three phase power charging and three-phase power discharging.

In both cases (single-phase and three-phase) is noted how the transition between Grid-Islanded and Grid-Connected mode is accomplished by employing the variable α_s, which determines the absence or presence of slack node (and the corresponding absence or presence of some constraints such as the droop control), the controller introduces this variable at each hour since it is assumed that all disconnections from the primary grid are intended and hence expected from some previous schedule. This variable could be assumed as stochastic to model sudden disconnections from the primary grid (such as failures); however, this is out of the scope of this document, and further investigation into the stochastic operation of the generic optimal power flow is required.

Chapter 4

Convex approximations

In this section, we present several approximations for solving the optimization problems presented in Chapter 3. Specifically, the second-order cone model presented in (Sepulveda et al., 2022a), the sequential convex approximation presented in (Sepulveda et al., 2022b), and the linear approximation based on Wirtinger calculus. The main idea is not to overwhelm the document but to illustrate different convex models that better behave in order to determine (see Chapter 5) the best one in order to escalate the problem (i.e., three-phase case, including a time of operation, model of BESS and, DGs) while reducing the computation effort.

4.1 Second-order cone approximation

Our models' non-convexity is mainly represented in two equations: the power balance and the norms associated with the voltage limits and the droop control. The first one is the power balance (4.1) due to the bilinear nature[1], namely:

$$\left(\mathbf{s}_k - \mathbf{s}_k^l\right)^* = \sum_{m \in \mathcal{N}} \mathbf{y}_{km} \mathbf{v}_k^* \mathbf{v}_m \tag{4.1}$$

This equation can be transformed by defining two new auxiliary variables: $\mathbf{h}_{km} = \mathbf{v}_k^* \mathbf{v}_m$ and, $u_k = \mathbf{v}_k^* \mathbf{v}_k = \|v_k\|^2$. These variables are substituted in

[1] In general, an equality constraint needs to be affine in order to be convex

(4.1). Then, it is possible to obtain (4.2).

$$\left(\mathbf{s}_k - \mathbf{s}_k^l\right)^* = \sum_{m \in \mathcal{N}} \mathbf{y}_{km} \mathbf{h}_{\mathbf{km}} \tag{4.2}$$

which corresponds to an affine equation and, non-linearity is absorbed by a new variable h. This variable is transformed into a hyperbolic relation, as given below:

$$\mathbf{h}_{km} = \mathbf{v}_k^* \mathbf{v}_m \tag{4.3}$$
$$\mathbf{h}_{km}\mathbf{h}_{km}^* = \mathbf{v}_k^* \mathbf{v}_m^* \mathbf{v}_m \mathbf{v}_m^* \tag{4.4}$$
$$\|\mathbf{h}_{km}\|^2 = \|\mathbf{v}_k\|^2 \|\mathbf{v}_m\|^2 \tag{4.5}$$
$$\|\mathbf{h}_{km}\|^2 = u_k u_m \tag{4.6}$$

Since it is a hyperbolic constraint, it could be rewritten as follows:

$$\|\mathbf{h}_{km}\| = \frac{1}{4}(u_k + u_m)^2 - \frac{1}{4}(u_k - u_m)^2 \tag{4.7}$$
$$(u_k - u_m)^2 + \|2\mathbf{h}_{km}\| = (u_k + u_m)^2 \tag{4.8}$$

This equation is still non-convex due to the equality relationship; a standard relaxation employs the inequality between both sides, which finally conduces to the convex expression below (Yuan and Hesamzadeh, 2018):

$$\left\| \begin{pmatrix} 2\mathbf{h}_{km} \\ u_k - u_m \end{pmatrix} \right\| \leq u_k + u_m \tag{4.9}$$

Which is a conic relaxation (Boyd and Vandenberghe, 2004). This equation jointly with (4.2) represents the second-order cone relaxation for the power flow, a visual representation of a second-order cone is given in Figure 4.1. Notice the interior of this cone is a convex set. However, the exact model is represented in the boundary of the set. In other words, the relaxation is exact iff the final solution belongs to the boundary of the second-order cone.

Another source of non-convexity is the norm presented in the droop control equation associated with the voltage control. For the sake of simplicity, we make use of the quadratic voltage droop controller presented in (Simpson-Porco et al., 2017). This strategy leads to the same steady-state as a classic droop controller; it transforms the droop voltage equation into an affine equation as follows:

$$h_{kk} - 1 = -\zeta_k (p_k^q - p_k^{\max}) \tag{4.10}$$

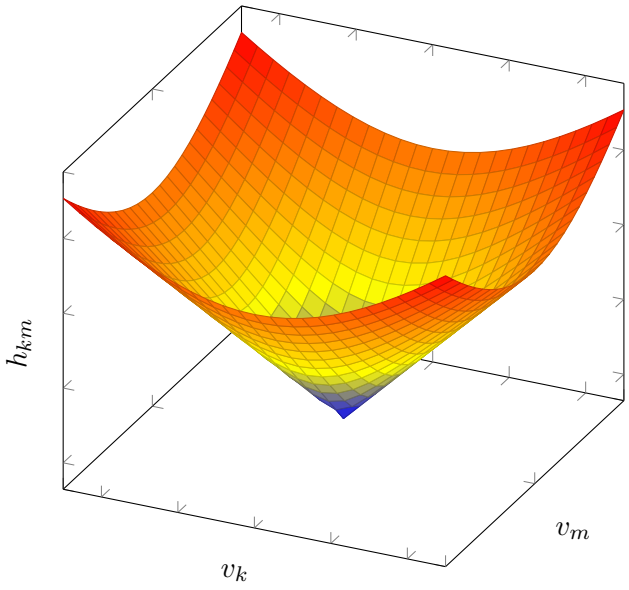

Figure 4.1: Representation of a Second Order Cone

Since the voltage variable has been transformed, the voltage deviation expressed in Equation (3.32) could be easily transformed as follows:

$$(v^{min})^2 \leq h_{kk} \leq (v^{max})^2 \tag{4.11}$$

The rest of the model, including variables and constraints, remains the same as in Chapter 3. The final model is convex with second-order cone constraints. This model was presented in (Sepulveda et al., 2022a).

4.2 Sequential convex optimization

For the foundations of sequential convex optimization (or sequential convex programming, SCP), we refer here to (Azhmyakov, 2019) and, (Duchi and Boyd, 2019). Consider an optimization problem (which does not necessarily need to be convex) as follows:

$$\begin{aligned} \min\ & f(u) \\ & g(u) \leq 0 \\ & h(u) = 0 \end{aligned} \tag{4.12}$$

The augmented optimization problem is defined by separating the variables and assuming that these are around the operating point. The idea is that the non-convex portions of the problem could be modeled (or approximated) by convex functions that are locally accurate, namely:

$$\begin{aligned} \min\ & f(u, \hat{u}) \\ & g(u, \hat{u}) \leq 0 \\ & h(u, \hat{u}) = 0 \\ & u = \hat{u} \end{aligned} \tag{4.13}$$

In this concept, the optimization model is solved partially by leveraging convex portions, and approximating (via iterations) the values $\hat{u}$ until some criteria of convergence is achieved. For the Optimal Power Flow case, a vector of nodal voltage as $\hat{v_k}$ and an auxiliary frequency as $\hat{\omega}$ are defined (Mhanna and Mancarella, 2022); with this variable, it is possible to introduce the frequency inside the Y_{bus}, and change the matrix in each iteration. The modified equations are presented below:

$$\left(\mathbf{s}_k - \mathbf{s}_k^l\right)^* = \sum_{m \in \mathcal{N}} \mathbf{y}_{km} \mathbf{v}_k^* \hat{\mathbf{v}}_m \tag{4.14}$$

$$\text{Real}\{v_k \hat{v_k}\} - 1 = -\zeta_k (p_k^g - p_k^{\max}) \tag{4.15}$$

where $\hat{v}$ is initially around the operation point of 1 p.u, and real$\{v_k \hat{v_k}\}$ indicates the real part of the product, since at each iteration some error is produced due to the slight difference between the constant $\hat{v_k}$ and the variable v_k. The main computation rule to solve the optimization model is described in Algorithm 1, presented in pseudocode. The partial (sequential) optimization problem is solved using conventional interior point methods.

The full structure of the sequential convex optimization for islanded grids was presented in (Sepulveda et al., 2022b). As deduced, this methodology has the main advantage of incorporating the variations of the frequency into the Y_{bus} at each iteration.

4.3 Wirtinger calculus

Equality constraints need to be affine in order to obtain a convex model. However, as observed from (4.1), the proposed model has a quadratic structure; furthermore, it does not follow the Cauchy-Riemann equations (Zill

Algorithm 1 Sequential convex optimization approach

Data: $Y_{\text{bus}}, p_k^{\max}, q_k^{\max}, c_k, q^{\min}, p^{\min}, \Delta\omega, v_k^{\min}, v_k^{\max}, \hat{v}, \hat{\omega}$
Result: v_k, ω
while *While* $\epsilon >$ *tolerance* **do**
  $(\mathbf{v_k}, \mathbf{s_k}, \omega) \leftarrow$ Solve Optimization model
  $\hat{\mathbf{v_k}} \leftarrow \mathbf{v_k}$
  $\epsilon \leftarrow \|\hat{\omega} - \omega\|$
  $\hat{\omega} \leftarrow \omega$
  $Y_{\text{bus}} \leftarrow A^\top \ \text{diag}(1/(r_{km} + j\hat{\omega}x_{km}))\ A$

and Shanahan, 2008), and hence it does not have derivative on the complex domain, preventing a Taylor approximation in the complex domain. However, Wirtinger Calculus allows to derivate of non-holomorphic functions similar to the conventional complex derivatives. Given a complex variable $\mathbf{z} = x + jy$ and a complex function $f(\mathbf{z}) = u + jv$, the Wirtinger calculus allows calculating its derivative and the conjugate derivative, as described in Equations (4.16) and (4.17).

$$\frac{\partial \hat{f}}{\partial z} = \frac{1}{2}\left(\frac{\partial u}{\partial x} + \frac{\partial v}{\partial y}\right) + \frac{j}{2}\left(\frac{\partial v}{\partial x} - \frac{\partial u}{\partial y}\right) \tag{4.16}$$

$$\frac{\partial \hat{f}}{\partial z^*} = \frac{1}{2}\left(\frac{\partial u}{\partial x} - \frac{\partial v}{\partial y}\right) + \frac{j}{2}\left(\frac{\partial v}{\partial x} + \frac{\partial u}{\partial y}\right) \tag{4.17}$$

It is possible to make linearization on the complex numbers for non-holomorphic functions based on the Wirtinger Calculus (Garces, 2021). The function $f(z)$ could be approximated as described in Equation (4.18).

$$f(z) = f(z_0) + \frac{\partial \hat{f}}{\partial z}\Delta z + \frac{\partial \hat{f}}{\partial z^*}\Delta z^* \tag{4.18}$$

The previous equation is very similar to the approximation for complex holomorphic functions. It is important to remark that (4.18) presents a slight abuse of the notation since, for some approximations, it is necessary to employ matrix calculus (Magnus, 2019) to obtain the derivatives for the equation power balance equation (in the three-phase case). A schematic representation of a linear approximation around the operation point is given in Figure 4.2

For the single-phase case, it is straightforward to make an approximation of equation (3.31) employing Wirtinger calculus and obtaining the equivalent

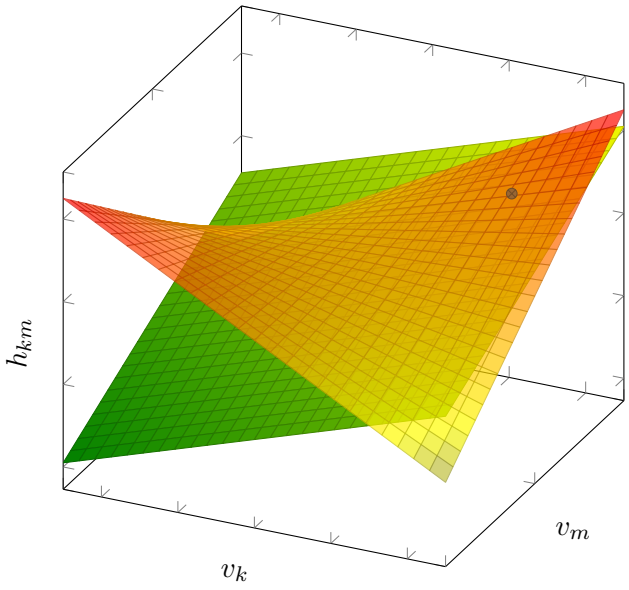

Figure 4.2: Representation of a linear approximation around and operation point.

equation as follows:

$$\left(\mathbf{s}_k - \mathbf{s}_k^l\right)^* = \sum_{m \in \mathcal{N}} \mathbf{y_{km}}(-\mathbf{1} + \mathbf{v_k} + \mathbf{v_m^*}) \tag{4.19}$$

And is possible to obtain a linear approximation employing Wirtinger Calculus for the voltage droop control as follows:

$$\frac{\mathbf{v_k} + \mathbf{v_k^*}}{\mathbf{2}} - \mathbf{1} = \zeta_k(p_k^g - p_k^{\max}) \tag{4.20}$$

For the three-phase case, it is necessary to make other types of approximations in order to manipulate properly (3.52), firstly, introduce a new variable defined as follows:

$$\mathbf{W} = \mathbf{V}\mathbf{V}^{\mathbf{H}} \tag{4.21}$$

where V^H performs the hermitian (conjugate transpose) of the vector V, for this reason W is a matrix (and the new source of non-convexity), and (3.52) could be rewritten as follows:

$$\mathbf{S_t^g} - \mathbf{S_t^d} \circ \alpha_\mathbf{t} = \text{diagonal}(\mathbf{Y}_{\text{bus}}^* \mathbf{W}) \tag{4.22}$$

Where the operator "diagonal" extracts the diagonal of a given matrix and form a column vector. Since W is the new source of non convexity, it could be approximated employing Wirtinger Calculus and Matrix calculus as follows:

$$\mathbf{W} \approx -\mathbf{V}^{\text{nom}}(\mathbf{V}^{\text{nom}})^{\mathbf{H}} + \mathbf{V}(\mathbf{V}^{\text{nom}})^{\mathbf{H}} + \mathbf{V}^{\text{nom}}(\mathbf{V})^{\mathbf{H}} \tag{4.23}$$

Which is an affine (and hence convex) equation. The voltage magnitude could be easily approximated as follows:

$$V_{k,f}^{m} = \|\mathbf{V}_{\mathbf{k},\mathbf{f}}\| \approx \frac{(\mathbf{V}_{\mathbf{k},\mathbf{f}}^{\text{nom}})^{*}\mathbf{V}_{\mathbf{k},\mathbf{f}} + \mathbf{V}_{\mathbf{k},\mathbf{f}}^{\text{nom}}(\mathbf{V}_{\mathbf{k},\mathbf{f}})^{*}}{\mathbf{2}(\sqrt{\mathbf{V}_{\mathbf{k},\mathbf{f}}^{\text{nom}}(\mathbf{V}_{\mathbf{k},\mathbf{f}}^{\text{nom}})^{*}})} \tag{4.24}$$

It is important to mention that $\|V_{k,a}\| = \|V_{k,b}\| = \|V_{k,c}\|$ for a given DG in the node k, and that all equations for the three-phase has been transformed into an affine equivalent except for equation (3.53), which remains quadratic and hence the final convex formulation is classified as a MIQP problem.

4.4 Effect of the frequency

As observed from section 3 the frequency is included in the droop control (3.42) and inside the $Y_{bus}(\omega)$. The maximum frequency variation allowed is $\Delta\omega = \pm 0.1Hz$. Hence, the model will also require disconnecting the charge to maintain the frequency inside its normal range of operation. Moreover, since the frequency reached for all converters requires being the same in the stationary state, the concept of frequency centroid is employed (3.48). It is straightforward to demonstrate that (3.42) and (3.48) could be transformed into the following equations:

$$\omega_o - \omega_{CI} = \xi_k(q_{k,t}^{g} - q_k^{\max}) \tag{4.25}$$

$$\omega_{CI} = \frac{\sum_{k\in\mathcal{N}} q_k^{\max} - q_{k,t}^{g}}{\sum_{k\in\mathcal{N}} \xi_k^{-1}} + \omega_o \tag{4.26}$$

These equations replace the ones mentioned earlier. Finally, it is possible to note that $omega_{CI}$ is the unified frequency of the Grid that all converters reach a stationary state. Furthermore, the value of ω_{CI} modifies the Y_{bus}.

In the present work, we do not consider the effect of the frequency on loads (for example, it is well-known that motors highly depend on the frequency of the Grid). This topic needs to be better explored for the Grid Islanded operation in the specialized literature, requiring further investigation.

Chapter 5

Results

5.1 Methodological framework

Different numerical experiments were carried out in order to answer the following questions:

- Is the inverse droop control suitable for grid with high r/x ratio?
- Is it necessary to include frequency inside the Y_{bus}?
- Which approximation is better to perform the OPF in grid islanded modes?

The data for radiance given in Figure 5.1 and, temperature given in Figure 5.2, were obtained from the web page (NASA, 2023) specifically for the Municipality of Riohacha, located in Colombia. Temperature coefficient k is assumed to be -0.005.

The data of the wind speed is depicted in Figure 5.3. It was also obtained from (NASA, 2023), for the Municipality of Riohacha. In the present work we assume a cut-in speed of $3m/s$ and a cut-out speed of $24m/s$ and a nominal speed of $15m/s$

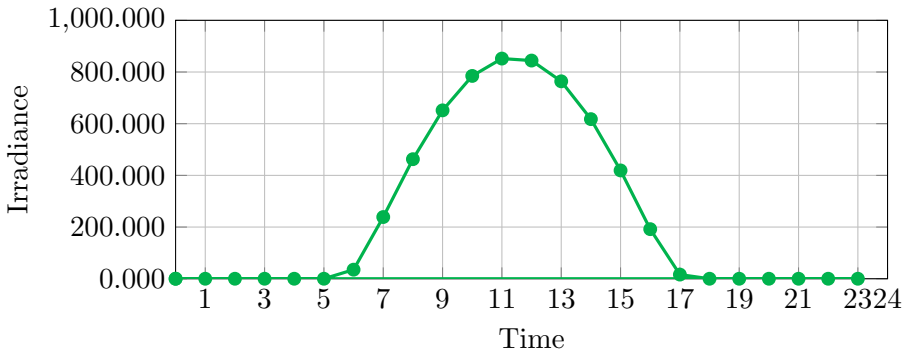

Figure 5.1: Irradiance in Riohacha for February First

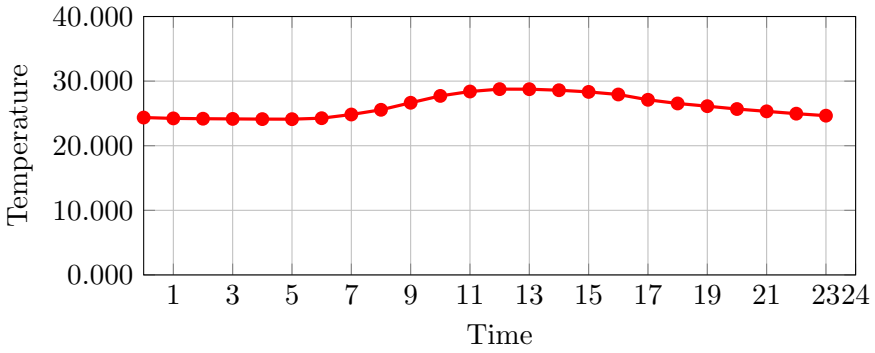

Figure 5.2: Temperature in Riohacha for February First

5.2 Variation of the Y_{bus} as function of the frequency

The static case is considered (this is, $t = 0$, and no presence of BESS), once solved these preliminary questions we are going to continue with the generic formulation described in previous sections. As stated before, the electric connections of the grid are represented by the matrix $\mathbf{Y}_{\text{bus}} \in \mathcal{C}^{n \times n}$ with entries $\mathbf{y}_{km}$. With a slight abuse of notation, this matrix can be represented as follows:

$$\mathbf{Y}_{\text{bus}} = A^{\top} \operatorname{diag}(1/\mathbf{z}_{km}) A \tag{5.1}$$

where A is the branch-to-node incidence matrix, and $\mathbf{z}_{km} = r_{km} +$

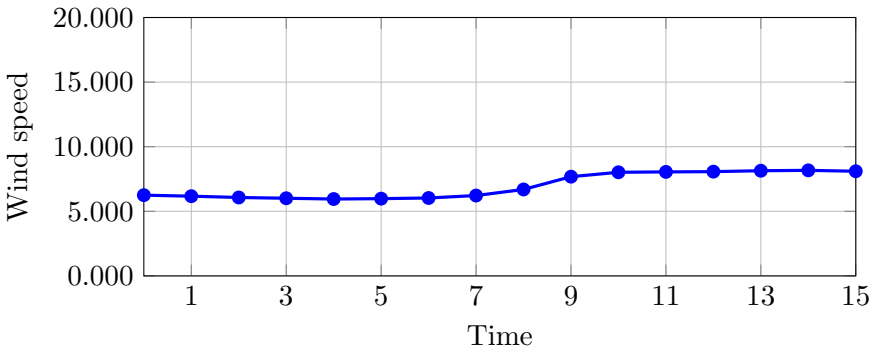

Figure 5.3: Wind speed in Riohacha for February First

$j\omega x_{km}, \forall km \in \mathcal{E}$. Recall that both ω and x_{km} are in per unit; thus, $\omega = 1+\Delta\omega$. Consider $\mathbf{z}^0_{km}$ and $\mathbf{Y}^0_{\text{bus}}$ as the values at nominal frequency (i.e., $\Delta\omega = 0$) and define a new variable ρ_{km} that fulfils the following expression:

$$\frac{1}{\mathbf{z}_{km}} = \frac{1}{\mathbf{z}^0_{km}} + \rho_{km} \tag{5.2}$$

Then, the admittance matrix may be represented as follows:

$$\mathbf{Y}_{\text{bus}} = \mathbf{Y}^0_{\text{bus}} + A^\top \operatorname{diag}(\rho_{km}) A \tag{5.3}$$

Therefore, the maximum variation of the admittance matrix (when a variation of the frequency is introduced) is obtained below:

$$\left\|\mathbf{Y}_{\text{bus}} - \mathbf{Y}^0_{\text{bus}}\right\| = \left\|A^\top \operatorname{diag}(\rho_{km}) A\right\| \leq \|A\|^2 \|\rho_{km}\| \tag{5.4}$$

Which means that the variation is bounded by the multiplication of the quadratic norm of the incidence matrix and ρ_{km}. From (5.2) the following expression is straightforward:

$$\rho_{km} = \frac{j(1-\omega)}{(r_{km}/x_{km} + j)(r_{km}/x_{km} + j\omega)} \tag{5.5}$$

Hence, $\|\rho_{km}\|$ can be easily bounded by replacing $\omega = 1+\Delta\omega$. Figure 5.4 shows the norm of ρ_{km} as function of the r_{km}/x_{km} ratio. As can be observed (and in conclusion) the variations in the Y_{bus} are slight when considering high r/x ratios. Therefore, although the frequency will be included as a variable

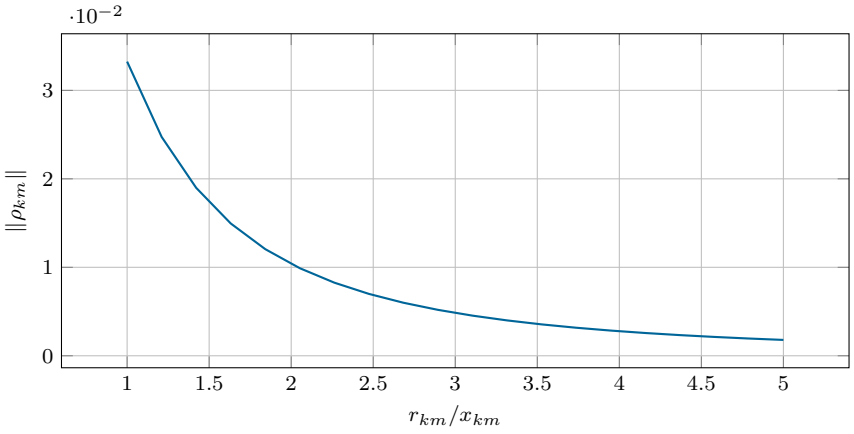

Figure 5.4: Norm of p_{km} with respect the r/x ratio

in the optimization algorithm, such variation might not be considerable in the Y_{bus}.

This theoretical analysis, p, is essential since it demonstrates that for grids with a high r/x ratio, it is not transcendent to include the frequency variation into the Y_{bus}, this could also be demonstrated numerically employing the sequential convex approximation since the frequency is included at each iteration, for instance, Table 5.1 illustrates the number of iterations, time of computation and frequency deviation. The average r/x ratio for each benchmark could be consulted in Table 5.2; notice that the benchmarks with a low r/x ratio (and a high number of nodes) are those whose frequency (and consequently, Y_{bus}) varies the most (although this variation is not significant compared to their nominal value of 60 Hz), although the benchmark 69 nodes have a high r/x mean ratio in comparison with 23 nodes, the first one has a large set of branches with a high x/r ratio (which is expected for long lines), and these are most susceptible to variations of frequency.

We could observe from Table 5.2 that the second-order cone approximation takes much more time of computation compared to the sequential approximation (even for the 100 nodes benchmark, the SOC does not converge).

Naturally, the computation time increases because of the number of nodes in a given benchmark and the number of iterations necessary for the convergence of the sequential optimization algorithm. As also happens

Table 5.1: General results of the proposed optimization model in others test systems.

Test system	Iterations	Time (s)	Frequency deviation (rad/s)
23 nodes	1	2.9671	0.0052
33 nodes	2	5.3634	0.0150
34 nodes	2	5.4130	0.0094
69 nodes	2	23.3643	0.186
100 nodes	3	53.2162	0.515

Table 5.2: Computation Times for Different test systems and mean r/x ratio

Test system	Mean r/x ratio	Time (s) Sequential Aprox.	Time (s) SOC
CIGRE (Rudion et al., 2006)	2.332	0.9700	5.270
23 nodes (Karimipour and Dinavahi, 2015)	1.804	2.9671	14.610
33 nodes (Zhu, 2002)	2.749	5.3634	31.470
34 nodes (Chis, 1997)	4.999	5.4130	31.076
69 nodes (Maheswarapu, 2011)	2.043	23.3643	127.580
100 nodes (Karimipour and Dinavahi, 2015)	1.473	53.2162	-

in the case of the CIGRE benchmark, since our initial point of frequency is around the nominal value (and the maximum deviation of frequency is usually low), the algorithm has a fast convergence (in terms of numbers of iterations), as stated in Figure 5.5, all benchmarks converge below the tolerance of 1×10^{-5}.

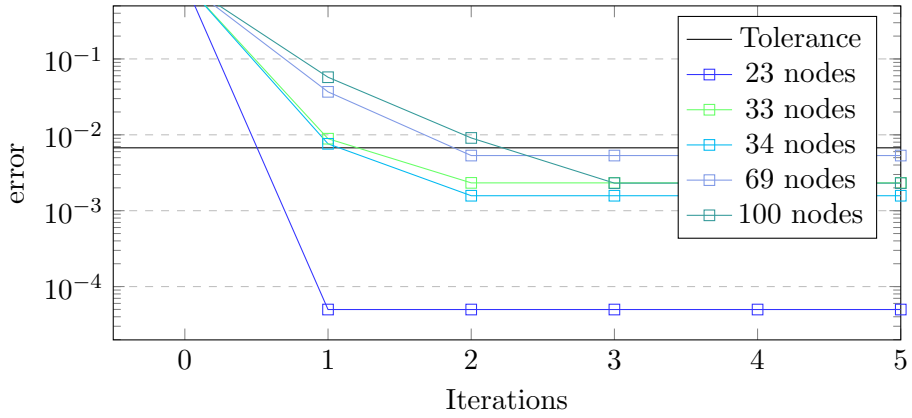

Figure 5.5: Convergence for different benchmarks.

It is also important to determine the variation of the Y_{bus} due to the changes in frequency. For the sake of simplicity, we analyse the norm of the variation against the nominal value, i.e., $\|Y^{o}_{\text{bus}} - Y^{iter}_{\text{bus}}\|$ (the applied norm is the well known Frobenius Norm). These results are presented in Figures 5.6 and 5.7.

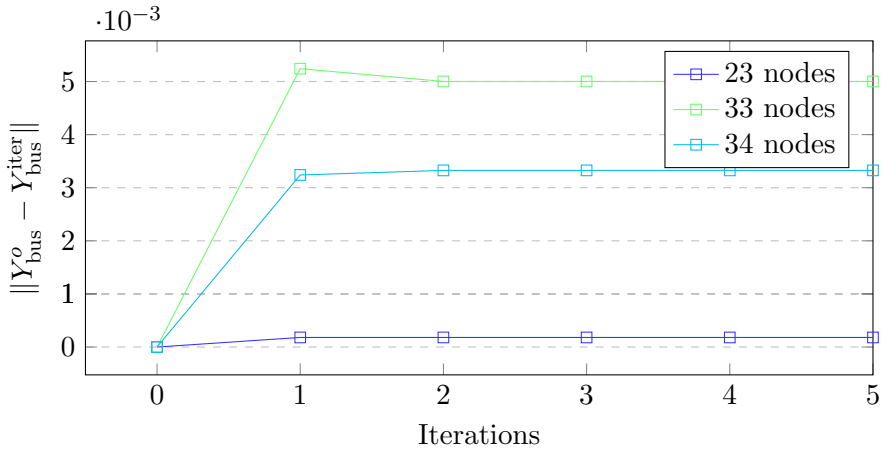

Figure 5.6: Variation of the Y_{bus} for the 23,33 and 34 nodes test systems.

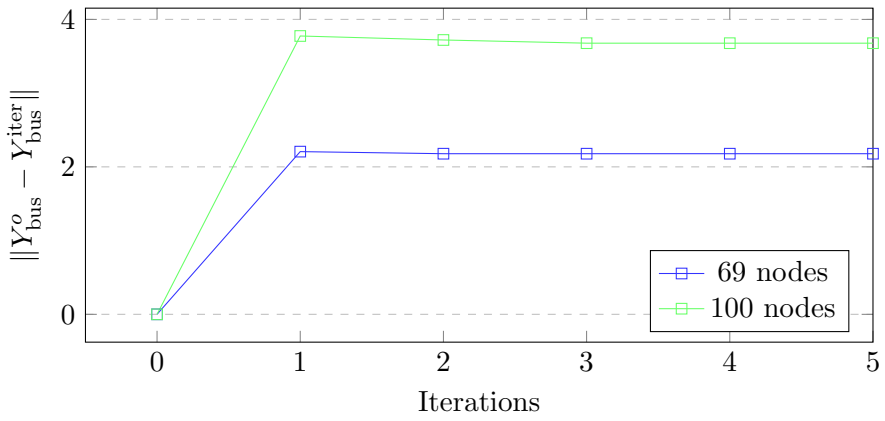

Figure 5.7: Variation of the Y_{bus} for the 69 and 100 nodes test systems.

It could be observed how the Y_{bus} variation of the first three test systems with respect to the frequency are negligible (in the order of 10^{-3}), and also how the Y_{bus} variate more (however this is very subjective, since, the Frobenius norm of the Y_{bus} at nominal frequency is in the order of 3×10^{2}

being the change of roughly 1.5%) for the case of the last two benchmarks.

In this preliminary analysis we demonstrated numerically that for grids with high r/x ratio, the droop inverse control is able to control the frequency around its nominal value, with acceptable values of deviation (this will be further discussed in the following sections for the dynamic cases), furthermore, some authors consider that a normal variation of the frequency during the operation horizon should be between $\pm\Delta 0.1$ Hz (that we achieve in the following sections were is analyzed the results for the single phase case and the three phase case). Moreover, we demonstrated both numerically and theoretically that it is not necessary to include the variation of the frequency into the Y_{bus} taking into account these grids with high r/x ratio and moreover the maximum frequency variation between $\pm\Delta 0.1$ Hz. Finally, from the two approximation discussed (SOC and Sequential) it could be concluded that the sequential approximation presents better performance in terms of computational time and scalability (high number of nodes).

5.3 Single phase case

From previous section it was observed how the sequential convex approximation presented in (Sepulveda et al., 2022b) performs better than the SOC approximation, however, it is important to mention that the first one is non-convex and, sometimes it behaves as a heuristic method that leverages by convex portions of NLP problems and approximate the solution depending on the starting point (Duchi and Boyd, 2019). Some authors such as (Mhanna and Mancarella, 2022) achieved to demonstrate conditions under that these type of sequential approximations are convex and guarantee global optimum (and hence uniqueness of the solution) for grid connected mode, however, for grid islanded mode there is no formal proof to rely on this approximation (more than numerically by comparing with other methods such as SOC), and hence this approximation was discarded and the Wirtinger approximation was opted to continue with the project. The results corresponding to the generic optimal power flow for the single phase case are presented in this section, the simulations were executed in CvxPy (Diamond and Boyd, 2016) a Python library that allows to write and solve convex optimization problems, and were solved employing (Gurobi Optimization, LLC, 2023) a solver specialized in convex (and mixed integer convex) programming. Several cases of study were performed as follows:

- Grid conected.
- Grid islanded.
  - Operation without BESS or PVs
  - Operation with BESS and PVs
- Generic operation with two disconnections from the main grid (11:00h - 13:00h) and (18:00h - 21:00h)

The benchmarks employed is the 33 nodes Test System described in (Zhu, 2002), the data concerning the modifications for the test system could be consulted in appendix A.

5.3.1 Connected mode

For the GC mode the slack node is always connected and hence it is not required to employ droop controls in order to maintain stable the Frequency and voltage, a normal power dispatch is performed seeking to minimize the costs of operation as observed in Figure 5.8, where the DGs are always dispatched (since it is cheaper than importing energy from the main grid) and the slack node is only employed during the second peak of demand since the available power of DGs is not full to supply all the load.

The behavior of the State of Charge of BESS is illustrated in Figure 5.9, where it could be observed how BESS charges during low demand in order to fully discharge during the peak of load where the energy purchase from the main grid is more expensive in order to reduce the overall costs of operation.

It is worth to state that all the PV units that were incorporated were dispatched at its maximum hourly power available since they operate at unitary factor and without any type of costs, however they are not included in Figures in order to not overwhelm the pictures (also due to their low contribution compared with DGs), this is important to mention in order to guarantee the repeatability of the optimization model.

5.3.2 Islanded mode

For the case of GI mode α_t^s is always 1, and hence, there is no presence of the slack node (and no frequency or voltage is imposed by the main grid),

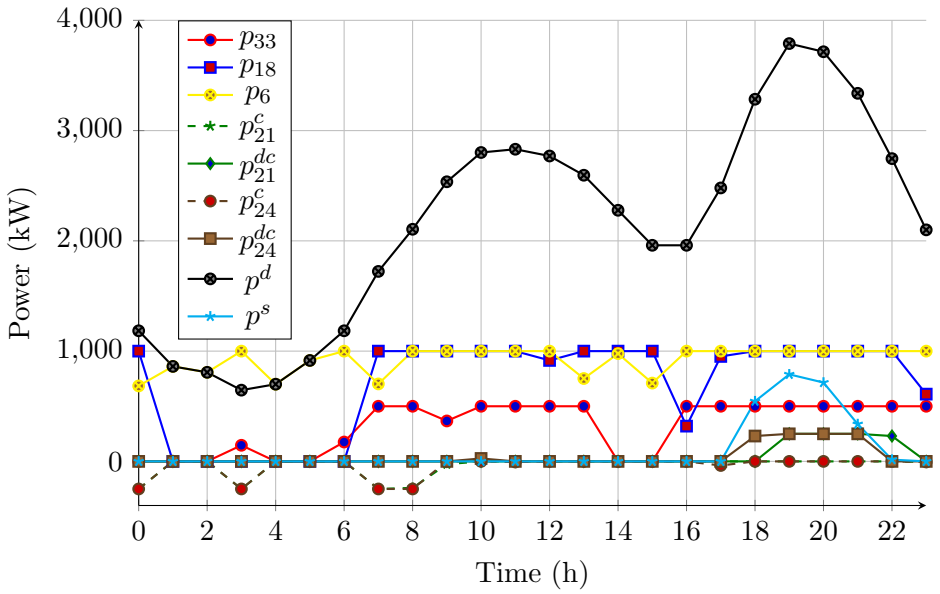

Figure 5.8: Power dispatch during full Grid-Connected (GC) mode.

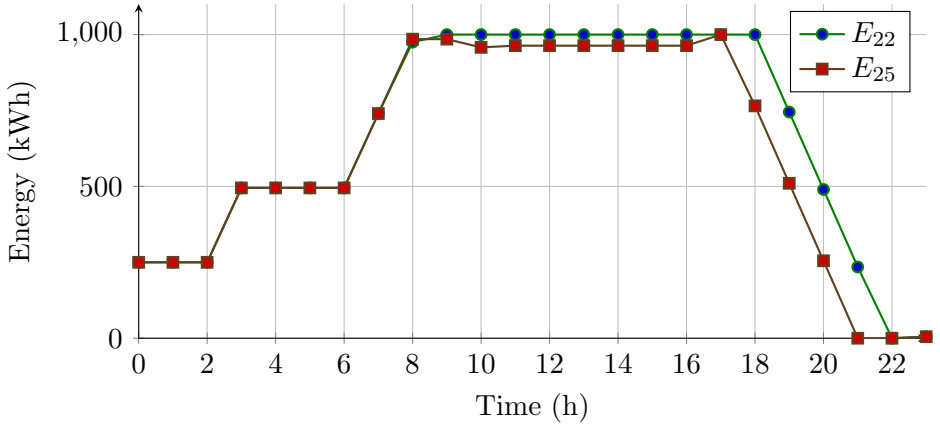

Figure 5.9: BESS energy during full Grid-Connected (GC) mode.

for this reason the DGs in the grid cease the constant generation and start regulating the voltage and frequency. The power dispatch for this case of study could be observed in Figure 5.10.

Where the dashed lines in Figure 5.8 represent the total load that the

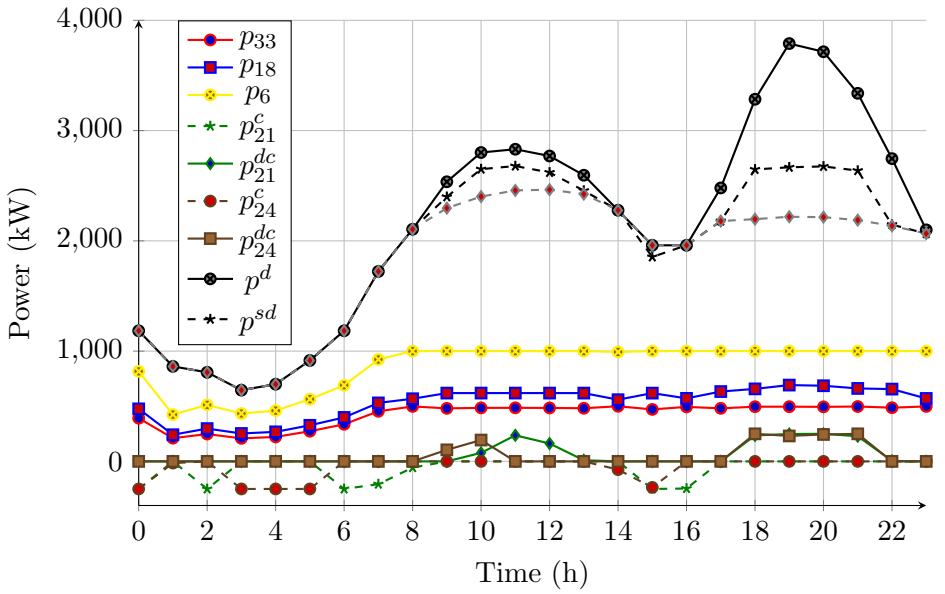

Figure 5.10: Power dispatch during full Grid-Islanded (GI) mode.

DGs can supply while maintaining the frequency and voltage within their normal range of operation, here we could observe how the presence of BESS reduces the noticeable amount of load shedding, especially during peak hours. This behaviour could be noticeable while analyzing the objective function (see table 5.3). Despite that the BESS reduces considerably the amount of load shedding and the costs of operation respectively, they do not affect considerably the frequency deviation as could be observed from Figure 5.14

Finally, the Energy stored by BESS could be observed in Figure 5.11 it is possible to note how contrary to the case were the slack is always connected, the BESS discharges once during the first peak of demand and recharges in order to fully discharge during the second peak of demand in order to reduce the amount of load shedding in these two peaks and consequently the costs of operation.

5.3.3 Generic operation

For the generic operation it is assumed two programmed disconnections from the main grid (11:00 - 13:00 and 18:00 -21:00, denoted for the semitranspar-

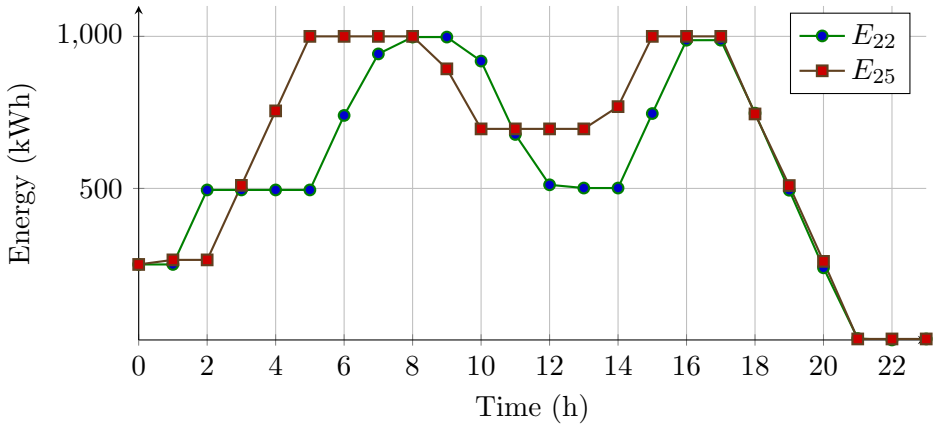

Figure 5.11: BESS energy during full Grid-Islanded (GI) mode.

ent red box), the power dispatch could be observed in Figure 5.12, where it could be noted how the amount of load shedding during the first disconnection is zero (contrary to the case of always GI operation), and that during the second disconnection the amount of load shedding is less than the GI case.

This could be specially explained from Figure 5.13 where it is possible to note that BESS are able to generate a depth discharge in the first peak (reducing to zero the load shedding during this time) and that thanks to the re-connection of the main grid they could be fully charged in order to fully discharge in the second peak of load.

The frequency response for the cases of study could be observed in Figure 5.14, it is possible to note that the frequency is always inside the range ($\pm\Delta 0.1$) and hence, the proposed optimization model ensures a safety value of frequency for the operation during the daily horizon. It is also interesting to observe the difference of the frequency values when there is presence of BESS and when there is not, the interesting part is that the frequency presents almost the same response, this is mainly due because this frequency is controlled with the reactive power of DGs and hence an active power injection does not affect considerable the response. Moreover, Figure 5.15 illustrates the voltages at the slack node for the four types of operation, and as discussed for the frequency, remains between the stable range of operation (around 10% of its nominal value).

Finally, table 5.3 illustrates the objective function results for the four

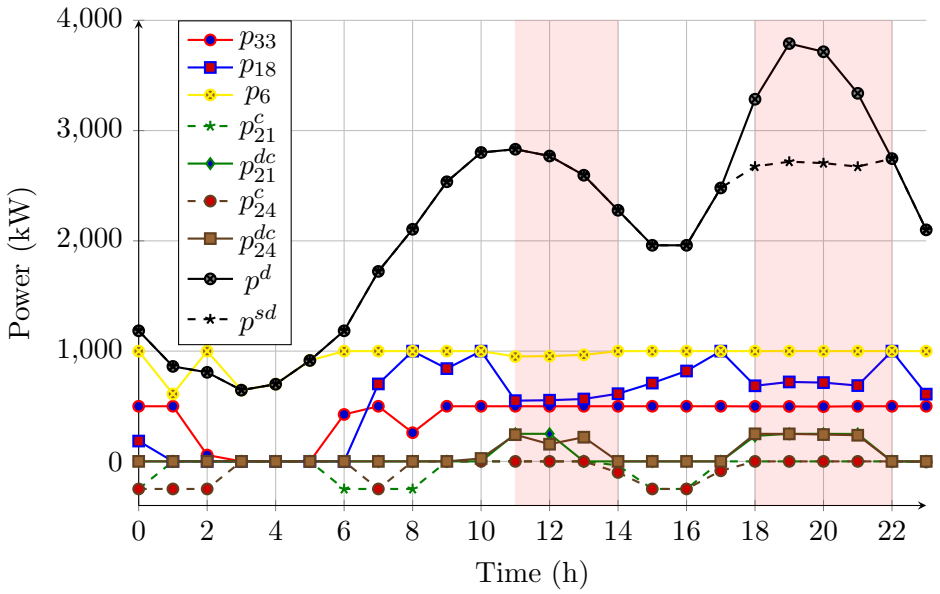

Figure 5.12: Power dispatch for the Generic Mode with two disconnections from the main grid.

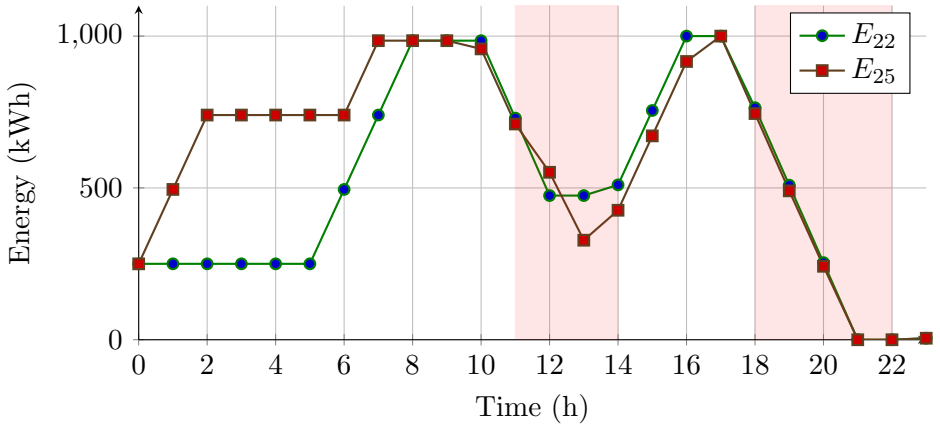

Figure 5.13: BESS energy for the generic mode with two disconnections from the main grid.

cases of operation. It could be observed how the inclusion of BESS in the grid islanded operation reduces considerable the costs of operation.

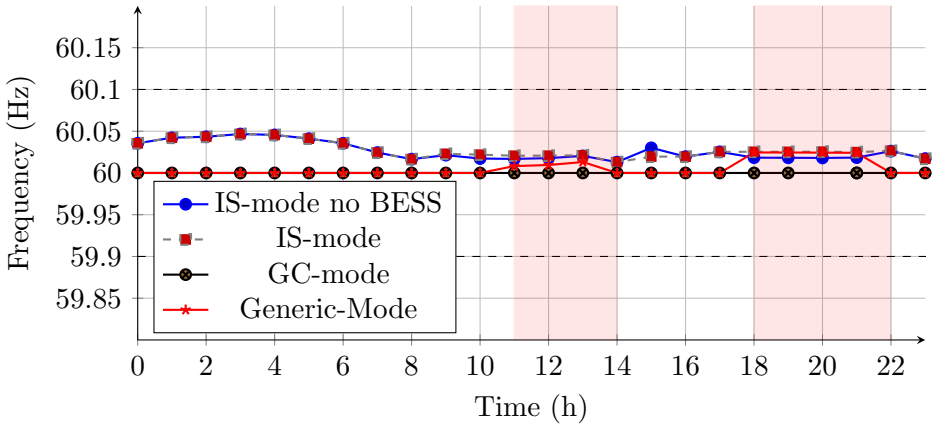

Figure 5.14: Frequency response during the different operation schemes

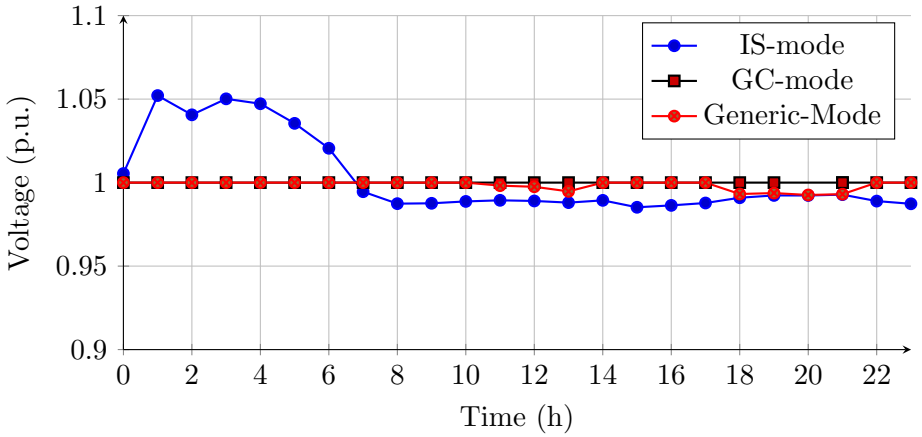

Figure 5.15: Voltage variation at the slack node during operation horizon

5.3.4 Extension to meshed grids

One of the main advantages of employing Bus Injection Formulations over Branch Flow model Formulations is the capability to be applied to meshed grids, for this reason we extend the Test System for the single phase meshed grid CIGRE benchmark (Rudion et al., 2006) (see appendix A for further details). For the sake of simplicity, we only consider the islanded operation of the grid ($\alpha = 1$).

Figure 5.16 represents the power dispatch for this test system where is ob-

Table 5.3: Value of the objective function for different operation modes

Type of operation	Obj. Function [k$]
GC-mode	1410.014
GI-mode	2546.740
GI-mode BESS	2243.235
Generic-mode	1901.773

served how (contrary to the 33 benchmark case study) this case needs more disconnection (after 8:00h) due to the capacity of DGs and total amount of load demanded in order to maintain stable the grid. Furthermore, BESS attempts to reduce the load shedding in the peaks of loads (11:00h-13:00h and 18:00h - 21:00h)

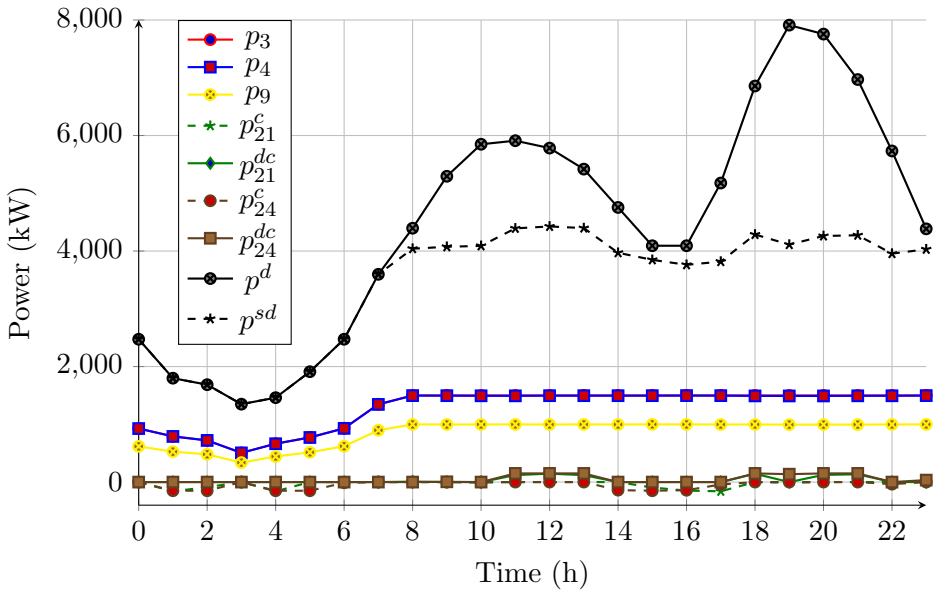

Figure 5.16: Power dispatch for CIGRE meshed grid during GI mode.

Finally, Figure 5.17 represents the frequency response for CIGRE benchmark, as stated there is not a great frequency deviation (the frequency is among its normal range of operation), this is thanks to the great amount of load shedding presented in Figure 5.16 (notice that, when a load is disconnected the reactive part is disconnected as well), which allows controlling properly the frequency by the reactive power of the DGs.

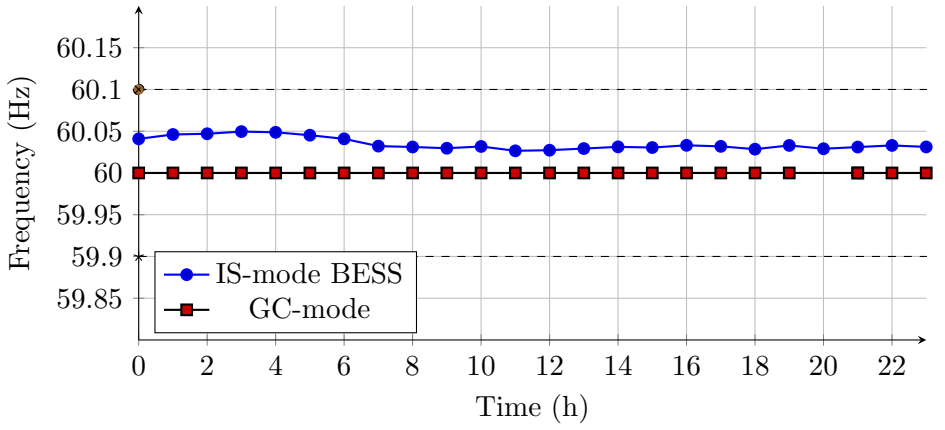

Figure 5.17: Frequency response for CIGRE meshed grid.

5.4 Three-Phase Case

For the three-phase case we make use of the Test System described in (Raju and Bijwe, 2008), it is a 25 node test system with nominal voltage of 4.16 kV and a nominal load of 3.3 MW. The data concerning the modifications effectuated to incorporate Distributed Energy Resources could be found in Appendix B. Once again, for the sake of simplicity and to make shorter the document, we only analyze the GI operation mode. of the three-phase case. The power dispatch could be observed in Figure 5.18.

The frequency response is illustrated in Figure 5.19, which is preserved between the safe range of operation.

The voltage profile for (t=0) and for (t=19) is observed in Figures 5.20 5.21, it is interesting to observe how in the nodes where DGs are installed (5,16,18) have the same voltage magnitude thanks to the restriction added in the three phase generic OPF. Now, it is important to ask: Why when there is surplus of generation the voltages and frequency deviates more? The question could be answered by observing the nature of the droop controllers (2.3) and (2.4), since there is surplus (more generation capacity than load) the right hand side deviates most (due to the difference between the nominal capacity of DGs and the capacity employed) and hence, the voltage or frequency deviates more as observed from the frequency responses of all the results and for the voltage at time t=0 observed in Figure 5.20.

However when there is deficit of generation the DGs are closer to their

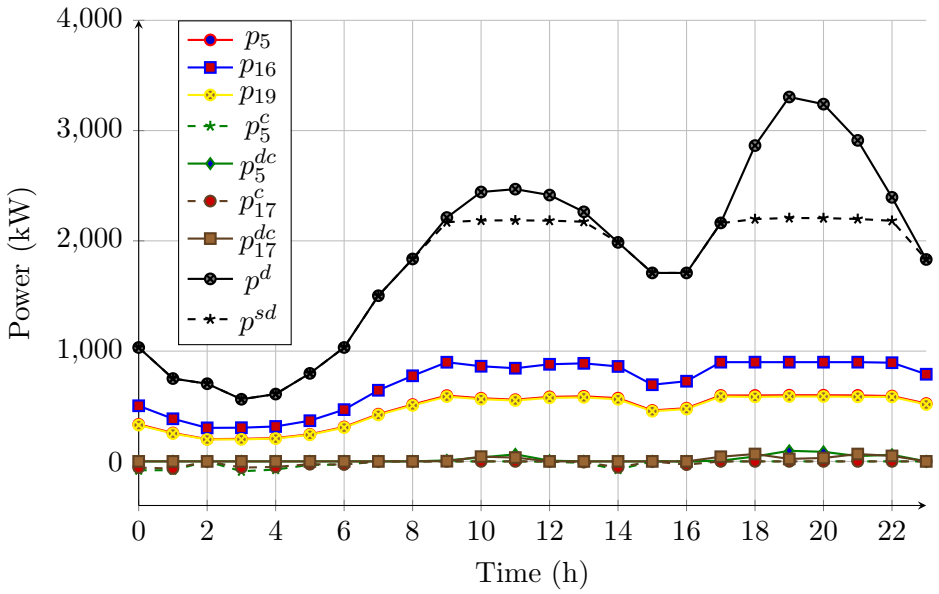

Figure 5.18: Power dispatch for GI operation three phase 25 nodes

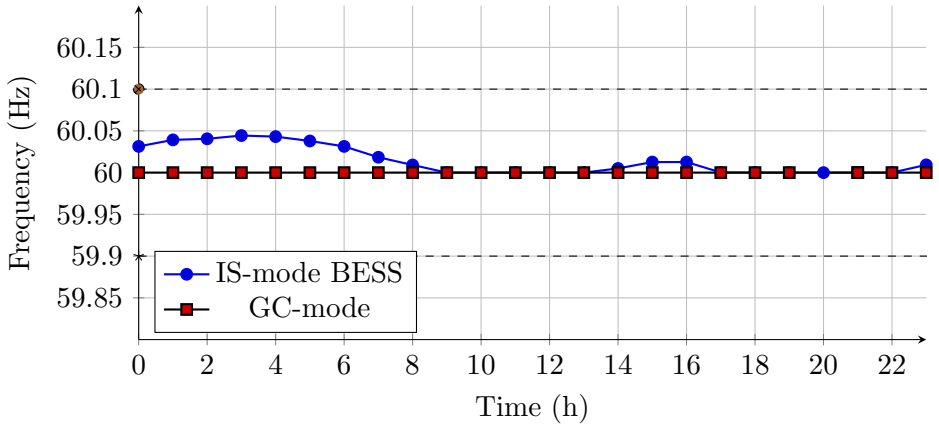

Figure 5.19: Frequency response for 25 nodes three phase benchmark during GI mode of operation

nominal capacity, and hence the right hand side of equations (2.3) and (2.4) is closer to zero, and consequently the frequency (and voltage as observed from Figure 5.21) is closer to its nominal value. To handle this problem some authors readjust (or incorporate into the optimization problem) the

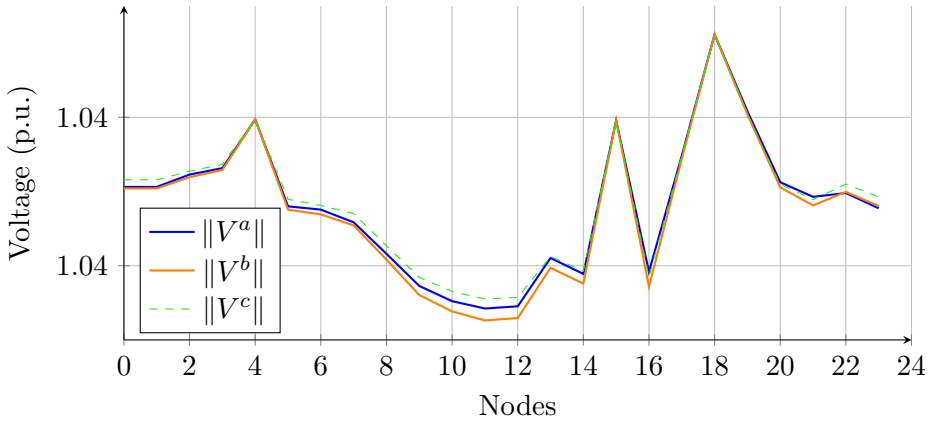

Figure 5.20: Voltage profiles at time t=0 for three phase GI mode of operation

constants associated with the droops (K_p and K_q) in order to minimize the response due to the overcapacity of generation, nevertheless, this is out of the scope of this document, and further investigation is required.

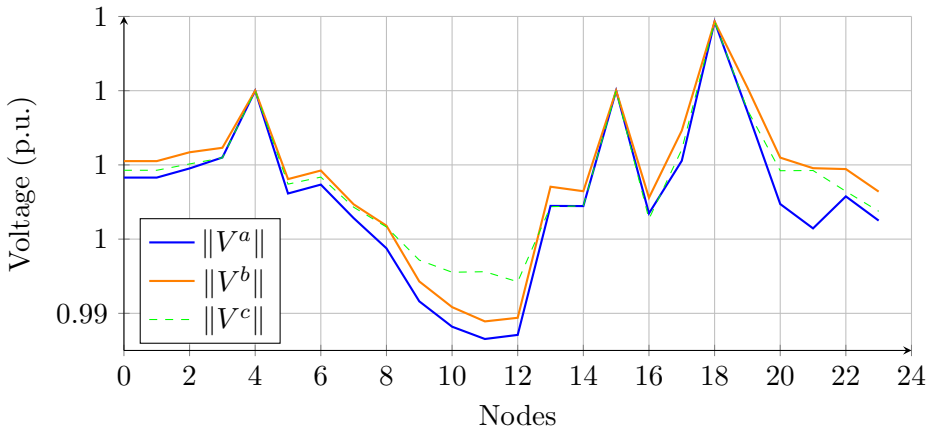

Figure 5.21: Voltage profiles at time t=19 for three phase GI mode of operation.

Chapter 6

Conclusions, discussion and future work

In this document, a unified framework for the optimal operation of active distribution networks has been presented. The proposed models include power flow equations, distributed generators, and battery-energy storage devices. Initially, the problem is a non-linear/non-convex problem, but it is convexified into an equivalent linear, quadratic, or second-order cone problem that is convex. Hence, a fast convergence, uniqueness of the solution, and global optimum are guaranteed. This optimization model could be executed during grid-islanded or grid-connected operations. The results demonstrated that the proposed methodology (which incorporates inverse droop controls due to the high r/x ratio) is suitable for the optimal operation of active distribution networks since it secures a safe operation (between a normal range) for variables such as frequency and voltage while minimizing the overall costs of operation. Several cases of studies were analyzed for single-phase, three-phase, radial, and meshed grids, demonstrating the scalability of the proposal.

From the three approximations presented, the Wirtinger approximation was preferred because it demonstrated high scalability; the second-order cone formulation takes much more time to converge (even without binary variables) depending on the number of nodes. Furthermore, it does not converge for the 100 nodes benchmark, having poor scalability; the main problem of the sequential convex optimization is that for grid-islanded operation, there is no formal proof to rely on, and hence this approximation is

classified as a Heuristic Method that depends on the starting point; furthermore, due to the combinatory explosion (high number of binary variables), this approximation would take much more time to converge in comparison to the Wirtinger Calculus. For this reason (and the preliminary analysis and single-phase case), the Wirtinger Calculus was employed for the general Optimal Power Flow for three-phase active distribution networks.

Including the frequency in the optimization problem allows for correctly operating the grid while securing a safe frequency variation range. During this work, we demonstrated that the inverse droop controller is suitable to control the frequency for grids with a high r/x ratio since it maintains the frequency between the operation range of $\pm 0.1Hz$. Moreover, it was demonstrated numerically and theoretically that for grids with a high r/x ratio, including the frequency inside the Y_{bus} is not transcendental since the variations due to the deviation of the frequency are negligible.

Finally, it demonstrated the versatility of the Generic Optimal Power Flow; it could be efficiently executed as a grid-connected or grid-islanded mode of operation or during both cases (Generic mode) when there is an intended (or scheduled) disconnection from the primary grid. For all cases, the main objective is the same, reducing the overall costs of operation while maintaining the grid's variables inside their normal range of operation; the most interesting case of study is the one related to the grid islanded operation since through load shedding it maintain stable the grid and provides the maximum amount of energy available from the DG units, in this case, the batteries are crucial in order to reduce the disconnection during the peak of loads (where it is assumed to be expensive to disconnect loads), this is more noticeable for the generic case when batteries present deep discharges during the first peak of load in order to reduce the load shedding thoroughly since the slack node could recharge the batteries during the hours between the peak of loads (13:00h-18:00h) in order to reduce the disconnection during the second peak of loads.

6.1 Future work

This document allows exploring new problems related to the generic (or Grid islanded) optimal power flow, for future works it would be important to:

- To take into account the stochastic nature of loads, distributed gener-

ators and the disconnection from the main grid α_s. This problem will complicate even more the formulation, since the load shedding and disconnection will become a stochastic parameter.

- to implement a distributed control; this proposal addressed the centralized control, however, it is important to analyze the possible advantages of distributed control specially for grid islanded ADNs, since this type of control is more reliable (but expensive) due to the immunity to single point failures.

- to implement a more detailed model of the grid, such as Transformers (and hence, primary and secondary distribution grid), On Load Tap Changers (OLTC) and Model of Loads that depend on the frequency. This proposal employed benchmarks for only the primary distribution grid (and hence without OLTC, transformers or without load models that depends on frequency) and hence, those models do not were employed.

- Implement a real life situation criteria or indexes of loads that could be disconnected, and do not rely on only in the cost of disconnection of the loads.

- Implement and compare in real life situations (or with simulation software products).

6.2 Applicability to the Colombian Case

In Colombia, non-conventional renewable energy resources were integrated into the grid with law 1715 of 2014 (CREG, 2014). This law aims to develop the penetration of distributed energy resources, especially those of renewable character, through their integration into the national market, participation of non-connected zones, reducing the environmental impact, and increasing demand.

Resolution CREG, 030 of 2018 (CREG, 2018b), intends to regulate operative and commercial aspects of DGs and auto generators connected to the grid to integrate Distributed energy resources effectively. Besides the regulatory part of the norm that finally forces the distribution operators to have geographical information of its utility open to the public and the corresponding location, capacity, and energy production of DGs, it contains some helpful information regarding the operation of the distribution

grid (those equations were initially presented by (Aguirre Colorado, 2020)). However, this resolution was corrected, rewritten, and represented by resolution CREG 174 of 2021 (CREG, 2021). It contains the procedure for the proper connection to the electrical grid and the corresponding guidelines for the settlement of surplus; Likewise, the steps to follow and the documentary requirements to be delivered according to the installed capacity and the type of generation are indicated in such regulation, they state that:

The sum of the installed power between DGs and Auto Generators could not exceed the fifty percent of the nominal capacity of the corresponding circuit, transformer, or substation where the connection has been requested. This could be mathematically written as:

$$\sum_{i=1}^{n} P_{gd,i}^{\text{nom}} + \sum_{s=1}^{m} P_{agd,s}^{\text{nom}} \leq 0.5 P_{\text{trafo}}^{\text{nom}} \tag{6.1}$$

Where $P_{gd,i}^{\text{nom}}$ is the maximum capacity of the Distributed Generators, $P_{agd,s}^{\text{nom}}$ is the maximum capacity of the auto generators and $P_{\text{trafo}}^{\text{nom}}$ is the maximum capacity of the transformer where the connection is requested.

The amount of energy that a given DG or Auto Generator could deliver to the grid, connected to the same circuit or transformer whose production of energy is different to a photovoltaic system, could not be greater than fifty percent of the average annual of hours with minimum diary demand.

$$\sum_{i=1}^{n} E_{gd,i} + \sum_{s=1}^{m} E_{agd,s} \leq 0.5 * \bar{D}_{\text{min}} \tag{6.2}$$

Where $E_{gd,i}$ is the energy injected of the Distributed Generators, $E_{agd,s}$ is the energy injected of the auto generators and $\bar{D}_{min}$ is the average annual of hours with minimum diary demand (in our case of study, the hour of minimum demand is presented at 3:00h, see appendix A).

The amount of energy that a given DG or Auto Generator could deliver to the grid, connected to the same circuit or transformer whose energy production is a photovoltaic system could not be greater than fifty percent of the average annual of hours with minimum diary demand between 6 a.m. and 6 p.m.

$$\sum_{i=1}^{n} E_{gd}^{pv} + \sum_{s=1}^{m} E_{agd}^{pv} \leq 0.5 * D_{min}^{-} \tag{6.3}$$

For this purpose, the resolution forces the distribution operators to have a geographical information system on their web page that illustrates if a given customer could deliver energy at a given time. For the non-connected zones (those who are not connected to the national power electric system), the usual way of supplying load is through diesel generators (which are very expensive to maintain) and only during some hours of the day, see (IPSE, 2022) for a complete review of the non-connected zones in Colombia, one line diagram, daily load curve and characteristics of the diesel generators. For these non-connected zones, resolution CREG (CREG, 2018c) regulates the amount of distributed or auto generators that could deliver a surplus of energy to the grid. In this case, it is 15% of the nominal capacity of the circuit in which they are connected, which corresponds to a slight modification of the right-hand side of equation (6.2).

Naturally, other regulatory aspects, mainly regarding commercial issues, such as Resolution CREG 015 of 2018 (CREG, 2018a), regulate the methodology for the remuneration of the Distribution activity. For example, *In the contracts of delivering surplus from the auto-generation or DGs, it is necessary to include a clause where the Distribution Operation must pay to a customer when the grid is not available to inject power.* However, in this work, we mainly focus on the operative aspects since they pose more problems to applying the methodology developed in this document, not the economic ones.

On the other hand, there are studies (project of resolution CREG 701 027 (CREG, 2023)) related to the control of the voltage by DGs or auto generators in order not to be charged. It states that:

The auto generators or DGs require implementing voltage control to maintain stable the voltage in the point of connection in a range between 0.9 to 1.1 p.u. of its corresponding nominal value. This control must allow the operation of the power factor between ± 0.9. This could be mathematically described as follows:

$$0.9 \leq V_{gd} \leq 1.1 \tag{6.4}$$

$$\text{power factor} = \frac{P_{gd}}{S_{gd}} \in \pm 0.9 \tag{6.5}$$

Moreover, the same regulation states that *DGs or auto generators that do not deliver surplus of energy to the grid, does not require participating in the voltage control.*

Considering all of these equations described and considerations, it is possible to incorporate them into the optimization problem and effectuate the generic Optimal Power Flow for the Colombian context. However, there are some technical problems described below:

- Despite equation (6.1) sets the maximum capacity of penetration of DGs to 50% of the capacity of transformer or circuit, equations (6.2)-(6.3) limits considerable the amount of surplus that could be delivered to the grid (around 10% of the nominal capacity of the primary grid from the case study presented in this document, see appendix A), and as observed from this document, it is necessary to allow a more significant injection of power from the DGs.

- Despite specifying the necessity of voltage control, CREG 701 027 does not specify if it is necessary to control the frequency from part of the DGs.

- All DGs and Auto generations require having anti-islanding protection when there is no service from the primary grid (see more in reference (CNO, 2022)), and hence they could not deliver a surplus of energy during Grid Islanded mode and only could consume the energy produced by themselves.

- Despite some incentives regarding the participation of customers in demand response during times of scarcity López-García et al. (2018), it is not clear in the short term if a central controller could disconnect and reconnect load in order to maintain stable a grid. Moreover, in the current resolutions, it is unclear if a central operator could control DGs or auto generators to manage the energy optimally in its grid (or even if a distribution operator could have its own DGs in its own grid).

This concise review regarding technical aspects regulated by CREG in Colombia allows concluding that this is a case where innovation collides with current regulation. The reserve of Colombia regulation avoiding high penetration of surplus of energy by DGs is understandable. The international case of Australia, where almost 1/3 of houses contain PV units, demonstrates problems regarding the stability of the grid and commercial aspects of distribution operators Hou et al. (2022). For this aspect, hosting capacity studies are necessary for the Colombian case to determine the distribution grid's fundamental capacity to receive Distributed Energy Resources. Moreover, it is necessary to explore other alternatives to supply energy for the non-connected zones (in order to reduce the cost of energy from non-connected zones), such as the one described in the document, which has been demonstrated to be effective in securing a safe range of operation for variables such as voltage and frequency while reducing the costs of operation and supplying the maximum amount of customers.

Appendix A

Data for single phase case

The network employed for testing the generic optimal power flow is the 33 nodes benchmark described in (Zhu, 2002). This grid has a nominal voltage of 12.66kV and a total nominal load of 3.715 MW. In order to effectuate the optimal operation for a given day, the following modifications were carried: BESS, DG units, and PV information is supplied in Tables A.1,A.2 and A.3, respectively. Furthermore, Figure A.1 represents the daily load variation.

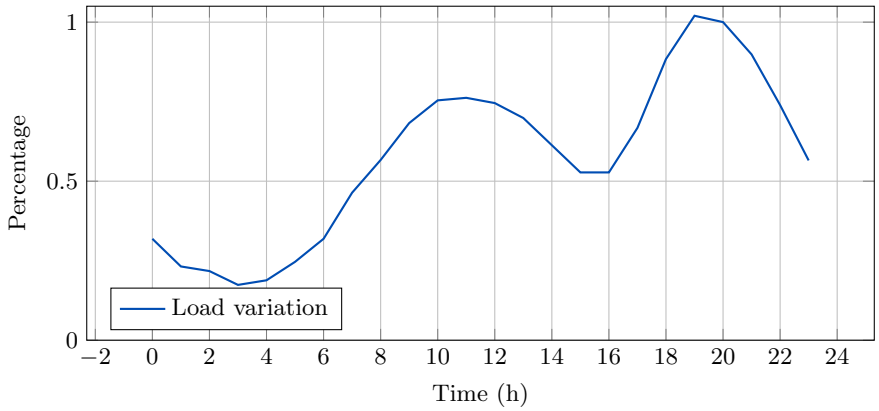

Figure A.1: Load curve for a daily operation

For the meshed case, we employed the CIGRE MV benchmark described in (Rudion et al., 2006). This benchmark of 4.16 kV of nominal voltage contains 11 nodes, in order to include DGs, the following modifications were performed: since the load in the first node is roughly 2.2 times the sum of

Table A.1: BESS information

Node	$E_{\min}$ [kWh]	$E_{\max}$ [kWh]	η	$P_{\max}$ [kW]
22	0	1000	0.95	250
25	0	1000	0.98	250

Table A.2: DGs information

Node	$p_{\min}$ [kW]	$p_{\max}$ [kW]	$q_{\min}$ [kVAr]	$q_{\max}$ [kVAr]	c_g [$/kWh]
6	0	1000	-200	200	254.167
18	0	1000	-200	100	266.132
33	0	500	-200	200	266.132

Table A.3: PV units data

Node	$pv^{\max}$ [kW]
2	80
22	80
25	20

all the loads of the grid (without taking into account the first node), all loads (except those of first node) are multiplied by 5 in order to have more consistently loads. The BESS, DG units, and PV information are given in Tables A.4,A.5 and A.6 respectively. For the sake of simplicity, the load variation is the same as Figure A.1.

Table A.4: BESS information

Node	$E_{\min}$ [kWh]	$E_{\max}$ [kWh]	η	$P_{\max}$ [kW]
2	0	600	0.95	150
10	0	400	0.95	160

For both benchmarks the ζ_k and ξ_k constants of the DG units are calculated modifying the equations presented in (Vergara et al., 2019a) as follows:

Table A.5: DGs information

Node	$p_{\min}$ [kW]	$p_{\max}$ [kW]	$q_{\min}$ [kVAr]	$q_{\max}$ [kVAr]	c_g [$/kWh]
3	0	1500	-400	800	532.262
4	0	1500	-250	600	406.84
8	0	1000	-100	500	490.4

Table A.6: PV units data

Node	$pv^{\max}$ [kW]
2	80
7	20
10	40

$$\zeta_k = \frac{\Delta v}{2p^{\max}} \tag{A.1}$$

$$\xi_k = \frac{\Delta \omega}{q^{\max}} \tag{A.2}$$

The maximum deviation of the frequency allowed is $\Delta\omega = 0.1Hz$ and the maximum deviation of the voltage allowed is 10% of its nominal value (which depends on the test system).

Appendix B

Data for three-phase case

We use the Test System described in (Raju and Bijwe, 2008) for the three-phase case. It is a 25-node test system with a nominal voltage of 4.16 kV and a nominal load of 3.3 MW. In order to effectuate the optimal operation for a given day, the following incorporation was carried: BESS, DG units, and PV, whose information is supplied in Tables B.1,B.2 and B.3, respectively. Furthermore, Figure B.1 represents the daily load variation.

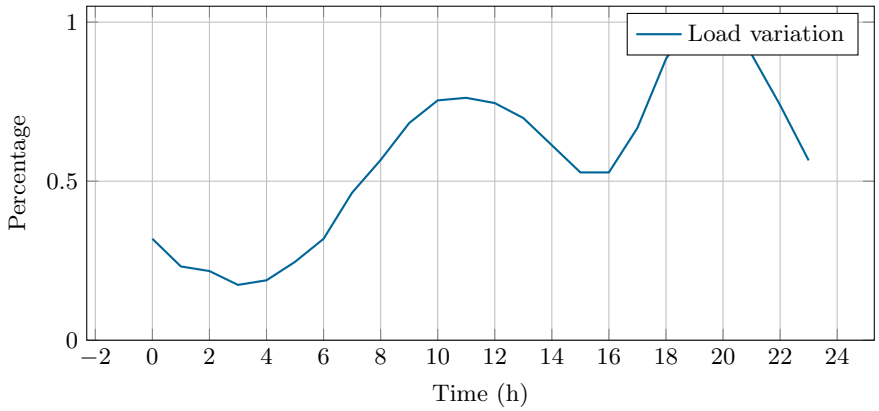

Figure B.1: Load curve for a daily operation

The maximum deviation of the frequency allowed is $\Delta\omega = 0.1Hz$ and the maximum deviation of the voltage allowed is 10% of its nominal value (which depends on the test system). And constants ζ_k and ξ_k are calcullated as follows:

Table B.1: BESS information

Node	$E_{\min}$ [kWh]	$E_{\max}$ [kWh]	η	$P_{\max}$ [kW]
5	100	750	0.98	100
17	50	500	0.98	100

Table B.2: DGs information

Node	$p_{\min}$ [kW]	$p_{\max}$ [kW]	$q_{\min}$ [kVAr]	$q_{\max}$ [kVAr]	c_g [$/kWh]
5	0	600	-200	500	254.167
16	0	900	-300	700	266.132
19	0	600	-200	400	266.132

Table B.3: PV units data

Node	$pv^{\max}$ [kW]
3	40
14	20
17	80

$$\zeta_k = \frac{\Delta v}{2p^{\max}} \tag{B.1}$$

$$\xi_k = \frac{\Delta \omega}{q^{\max}} \tag{B.2}$$

Bibliography

Abdelaziz, M. M. A., Farag, H. E., El-Saadany, E. F., and Mohamed, Y. A.-R. I. (2013). A novel and generalized three-phase power flow algorithm for islanded microgrids using a newton trust region method. *IEEE Transactions on Power Systems*, 28(1):190 – 201. Cited by: 269.

Abdi, H., Beigvand, S. D., and Scala, M. L. (2017). A review of optimal power flow studies applied to smart grids and microgrids. *Renewable and Sustainable Energy Reviews*, 71:742–766.

Aguirre Colorado, D. (2020). Evaluación de normas de fuentes no convencionales de energía renovable en colombia para la determinación de índices de conexión.

Alqunun, K., Guesmi, T., and Farah, A. (2020). Load shedding optimization for economic operation cost in a microgrid. *Electrical Engineering*.

Ansari, S., Chandel, A., and Tariq, M. (2021). A comprehensive review on power converters control and control strategies of ac/dc microgrid. *IEEE Access*, 9:17998–18015.

Axler, S. (2015). *Operators on Inner Product Spaces*, pages 203–240. Springer International Publishing, Cham.

Azhmyakov, V. (2019). *A Relaxation-Based Approach to Optimal Control of Hybrid and Switched Systems*. Elsevier.

Bassey, O., Chen, C., and Butler-Purry, K. L. (2021). Linear power flow formulations and optimal operation of three-phase autonomous droop-controlled microgrids. *Electric Power Systems Research*, 196:107231.

Bedoya, J. C., Abdelhadi, A., Liu, C.-C., and Dubey, A. (2019). A qcqp and sdp formulation of the optimal power flow including renewable en-

ergy resources. In *2019 International Symposium on Systems Engineering (ISSE)*, pages 1–8.

Boyd, S. and Vandenberghe, L. (2004). *Convex optimization*. Cambridge university press.

Bravo-López, M.-F., Garcés, A., and Mora-Flórez, J.-J. (2021). Simplified dynamic models for three-phase microgrids. *International Transactions on Electrical Energy Systems*, 31(2):e12742.

Capitanescu, F. (2016). Critical review of recent advances and further developments needed in ac optimal power flow. *Electric Power Systems Research*, 136:57–68.

Chis, M. (1997). Capacitor placement in distribution systems using heuristic search strategies. *IEE Proceedings - Generation, Transmission and Distribution*, 144:225–230(5).

CNO (2022). CNO 1522 of 2022.

Costa, A. D., Haffner, S., Resener, M., Pereira, L. A., and Ferraz, B. M. P. (2020). *Linear Model to Represent Unbalanced Distribution Systems in Optimization Problems*, pages 69–120. Springer International Publishing, Cham.

CREG (2014). Law 1715 of 2014.

CREG (2018a). Resolution 015 of 2018.

CREG (2018b). Resolution 030 of 2018.

CREG (2018c). Resolution 038 of 2018.

CREG (2021). Resolution 174 of 2021.

CREG (2023). Project of resolution 701 of 2023.

Diamond, S. and Boyd, S. (2016). CVXPY: A Python-embedded modeling language for convex optimization. *Journal of Machine Learning Research*, 17(83):1–5.

Dragičević, T. (2018). Model predictive control of power converters for robust and fast operation of ac microgrids. *IEEE Transactions on Power Electronics*, 33(7):6304–6317.

Dragičević, T., Vazquez, S., and Wheeler, P. (2021). Advanced control methods for power converters in dg systems and microgrids. *IEEE Transactions on Industrial Electronics*, 68(7):5847–5862.

Duchi, J. and Boyd, S. (2019). Sequential convex programming. https://web.stanford.edu/class/ee364b/lectures/seq_notes.pdf.

Díaz, G., Gómez-Aleixandre, J., and Coto, J. (2016). Direct backward/forward sweep algorithm for solving load power flows in ac droop-regulated microgrids. *IEEE Transactions on Smart Grid*, 7(5):2208–2217.

Engelmann, A., Jiang, Y., Muhlpfordt, T., Houska, B., and Faulwasser, T. (2019). Toward distributed opf using aladin. *IEEE Transactions on Power Systems*, 34(1):584–594.

Engelmann, A., Mühlpfordt, T., Jiang, Y., Houska, B., and Faulwasser, T. (2017). Distributed ac optimal power flow using aladin. *IFAC-PapersOnLine*, 50(1):5536–5541. 20th IFAC World Congress.

Gan, L. and Low, S. H. (2014). Convex relaxations and linear approximation for optimal power flow in multiphase radial networks. In *2014 Power Systems Computation Conference*, pages 1–9.

Garces, A. (2020). Small-signal stability in island residential microgrids considering droop controls and multiple scenarios of generation. *Electric Power Systems Research*, 185:106371.

Garces, A. (2021). *Optimal power flow*, chapter 10, pages 171–193. John Wiley and Sons, Ltd.

Garcés Ruiz, A. (2020). Optimización convexa: aplicaciones en operación y dinámica de sistemas de potencia.

Garcès, A. and Gil-Gonzàlez, W. (2021). Stability analysis for a grid-forming converter with inverse droop connected to an infinite bus. In *2021 IEEE 5th Colombian Conference on Automatic Control (CCAC)*, pages 286–290.

García-Ceballos, C., Pérez-Londoño, S., and Mora-Flórez, J. (2021). Integration of distributed energy resource models in the vsc control for microgrid applications. *Electric Power Systems Research*, 196:107278.

Gil-González, W., Montoya, O. D., Holguín, E., Garces, A., and Grisales-Noreña, L. F. (2019). Economic dispatch of energy storage systems in dc microgrids employing a semidefinite programming model. *Journal of Energy Storage*, 21:1–8.

Groppi, D., Pfeifer, A., Garcia, D. A., Krajačić, G., and Duić, N. (2021). A review on energy storage and demand side management solutions in smart energy islands. *Renewable and Sustainable Energy Reviews*, 135:110183.

Guerrero, J. M., Vasquez, J. C., Matas, J., de Vicuna, L. G., and Castilla, M. (2011). Hierarchical control of droop-controlled ac and dc microgrids—a general approach toward standardization. *IEEE Transactions on Industrial Electronics*, 58(1):158–172.

Gurobi Optimization, LLC (2023). Gurobi Optimizer Reference Manual.

Hemmatpour, M. H., Mohammadian, M., and Gharaveisi, A. A. (2016). Optimum islanded microgrid reconfiguration based on maximization of system loadability and minimization of power losses. *International Journal of Electrical Power and Energy Systems*, 78:343–355.

Hou, Y., Liu, M. Z., and Ochoa, L. F. (2022). Residential pv hosting capacity, voltage unbalance, and power rebalancing: An australian case study. In *2022 IEEE PES Innovative Smart Grid Technologies Conference Europe (ISGT-Europe)*, pages 1–5.

Huang, Y., Ju, Y., Ma, K., Short, M., Chen, T., Zhang, R., and Lin, Y. (2022a). Three-phase optimal power flow for networked microgrids based on semidefinite programming convex relaxation. *Applied Energy*, 305:117771.

Huang, Y., Ju, Y., Ma, K., Short, M., Chen, T., Zhang, R., and Lin, Y. (2022b). Three-phase optimal power flow for networked microgrids based on semidefinite programming convex relaxation. *Applied Energy*, 305:117771.

IPSE (2022). monthly telemetry report.

Ja'afreh, O., Siam, J., and Shehadeh, H. (2022). Power loss and total load demand coverage in stand-alone microgrids: A combined and conventional droop control perspectives. *IEEE Access*, 10:128721–128731.

Karimipour, H. and Dinavahi, V. (2015). Parallel domain decomposition based distributed state estimation for large-scale power systems. In *2015 IEEE/IAS 51st Industrial and Commercial Power Systems Technical Conference (I and CPS)*, pages 1–5.

Kersting, W. (2017). *Distribution System Modeling and Analysis*. CRC Press.

Khayat, Y., Shafiee, Q., Heydari, R., Naderi, M., Dragičević, T., Simpson-Porco, J. W., Dörfler, F., Fathi, M., Blaabjerg, F., Guerrero, J. M., and Bevrani, H. (2020). On the secondary control architectures of ac microgrids: An overview. *IEEE Transactions on Power Electronics*, 35(6):6482–6500.

Kreishan, M. Z. and Zobaa, A. F. (2021). Optimal allocation and operation of droop-controlled islanded microgrids: A review. *Energies*, 14(15).

Kryonidis, G. C., Kontis, E. O., Papadopoulos, T. A., Pippi, K. D., Nousdilis, A. I., Barzegkar-Ntovom, G. A., Boubaris, A. D., and Papanikolaou, N. P. (2021). Ancillary services in active distribution networks: A review of technological trends from operational and online analysis perspective. *Renewable and Sustainable Energy Reviews*, 147:111198.

Lavaei, J. and Low, S. H. (2012). Zero duality gap in optimal power flow problem. *IEEE Transactions on Power Systems*, 27(1):92–107.

Liu, D., Zhang, C., and Dong, Z. (2019). Stochastic optimal power flow for islanded microgrids considering droop control. In *2019 IEEE Innovative Smart Grid Technologies - Asia (ISGT Asia)*, pages 3156–3161.

Low, S. H. (2014). Convex relaxation of optimal power flow—part ii: Exactness. *IEEE Transactions on Control of Network Systems*, 1(2):177–189.

López-García, D., Arango-Manrique, A., and Carvajal-Quintero, S. X. (2018). Integración de los recursos energéticos distribuidos en microrredes aisladas: paradigma colombiano. *TecnoLógicas*, 21(42):13–30.

Macedo, L. H., Franco, J. F., Rider, M. J., and Romero, R. (2015). Optimal operation of distribution networks considering energy storage devices. *IEEE Transactions on Smart Grid*, 6(6):2825–2836.

Magnus, J. R. (2019). *Matrix Differential Calculus with Applications in Statistics and Econometrics*. Wiley.

Maheswarapu, S. (2011). Enhancement of voltage profile and loss minimization in distribution systems using optimal placement and sizing of power system modeled dgs.

Masters, G. M. (2004). *Wind Power Systems*, chapter 6, pages 307–383. John Wiley and Sons, Ltd.

Maulik, A. and Das, D. (2018). Optimal operation of droop-controlled islanded microgrids. *IEEE Transactions on Sustainable Energy*, 9(3):1337–1348.

Mhanna, S. and Mancarella, P. (2022). An exact sequential linear programming algorithm for the optimal power flow problem. *IEEE Transactions on Power Systems*, 37(1):666–679.

Mishra, D. K., Ghadi, M. J., Azizivahed, A., Li, L., and Zhang, J. (2021). A review on resilience studies in active distribution systems. *Renewable and Sustainable Energy Reviews*, 135:110201.

Molzahn, D. K. and Hiskens, I. A. (2019). *A Survey of Relaxations and Approximations of the Power Flow Equations*. Now Foundations and Trends.

Montoya, O. D., Gil-González, W., and Molina-Cabrera, A. (2020). Second-order cone approximation for voltage stability analysis in direct-current networks. *Symmetry*, 12(10).

Mumtaz, F., Syed, M. H., Hosani, M. A., and Zeineldin, H. H. (2016). A novel approach to solve power flow for islanded microgrids using modified newton raphson with droop control of dg. *IEEE Transactions on Sustainable Energy*, 7(2):493–503.

NASA (2023). Ms windows nt kernel description. [Online]. Available from: https://power.larc.nasa.gov/data-access-viewer/. Accessed: 2023-30-01.

Olivares, D. E., Cañizares, C. A., and Kazerani, M. (2014). A centralized energy management system for isolated microgrids. *IEEE Transactions on Smart Grid*, 5(4):1864–1875.

Planas, E., de Muro, A. G., Andreu, J., Kortabarria, I., and Martínez de Alegría, I. (2013). General aspects, hierarchical controls and droop methods in microgrids: A review. *Renewable and Sustainable Energy Reviews*, 17:147–159.

Raju, G. and Bijwe, P. (2008). Efficient reconfiguration of balanced and unbalanced distribution systems for loss minimisation. *Generation, Transmission and Distribution, IET*, 2:7 – 12.

Ramirez, D.-A., Garcés, A., and Mora-Flórez, J.-J. (2021). A convex approximation for the tertiary control of unbalanced microgrids. *Electric Power Systems Research*, 199:107423.

Rios, M. A. and Garces, A. (2022). An optimization model based on the frequency dependent power flow for the secondary control in islanded microgrids. *Computers and Electrical Engineering*, 97:107617.

Risi, B.-G., Riganti-Fulginei, F., and Laudani, A. (2022). Modern techniques for the optimal power flow problem: State of the art. *Energies*, 15(17).

Rocabert, J., Luna, A., Blaabjerg, F., and Rodríguez, P. (2012). Control of power converters in ac microgrids. *IEEE Transactions on Power Electronics*, 27(11):4734–4749.

Rudion, K., Orths, A., Styczynski, Z., and Strunz, K. (2006). Design of benchmark of medium voltage distribution network for investigation of dg integration. In *2006 IEEE Power Engineering Society General Meeting*, pages 6 pp.–.

Saleh, M., Esa, Y., Hariri, M. E., and Mohamed, A. (2019). Impact of information and communication technology limitations on microgrid operation. *Energies*, 12(15).

Sepulveda, S., Garces, A., and Juan-Jose, M.-F. (2022a). Optimal operation of active distribution networks considering deficit of generation. In *2022 IEEE Power and Energy Society General Meeting (PESGM)*, pages 01–08.

Sepulveda, S., Garces, A., and Mora-Flórez, J. (2022b). Sequential convex optimization for the dynamic optimal power flow of active distribution networks. *IFAC-PapersOnLine*, 55(9):268–273. 11th IFAC Symposium on Control of Power and Energy Systems CPES 2022.

Sepúlveda, S., Ruíz, A. G., and Mora-Flórez, J. J. (2022). Optimal power flow for three-phase unbalanced active distribution networks with delta connections. In *2022 IEEE ANDESCON*, pages 1–6.

Sepúlveda García, S. and Garcés, A. (2022). Análisis de sensibilidad y estabilidad de pequeña señal en convertidores seguidores de red. *TecnoLógicas*, 25(54):e2383.

Sepúlveda-García, S., Montoya, O. D., and Garcés, A. (2022). Power flow solution in bipolar dc networks considering a neutral wire and unbalanced loads: A hyperbolic approximation. *Algorithms*, 15(10).

Shahgholian, G. (2021). A brief review on microgrids: Operation, applications, modeling, and control. *International Transactions on Electrical Energy Systems*, 31(6):e12885.

Simpson-Porco, J. W., Dörfler, F., and Bullo, F. (2017). Voltage stabilization in microgrids via quadratic droop control. *IEEE Transactions on Automatic Control*, 62(3):1239–1253.

Sorensen, K. (2015). Metaheuristics—the metaphor exposed. *International Transactions in Operational Research*, 22(1):3–18.

Stevenson, W. (1982). *Elements of Power System Analysis*. Electrical Power and Energy Series. McGraw-Hill.

Vergara, P. P., López, J. C., Rider, M. J., and da Silva, L. C. P. (2019a). Optimal operation of unbalanced three-phase islanded droop-based microgrids. *IEEE Transactions on Smart Grid*, 10(1):928–940.

Vergara, P. P., López, J. C., Rider, M. J., Shaker, H. R., da Silva, L. C., and Jørgensen, B. N. (2020). A stochastic programming model for the optimal operation of unbalanced three-phase islanded microgrids. *International Journal of Electrical Power and Energy Systems*, 115:105446.

Vergara, P. P., Rey, J. M., López, J. C., Rider, M. J., da Silva, L. C., Shaker, H. R., and Jørgensen, B. N. (2019b). A generalized model for the optimal operation of microgrids in grid-connected and islanded droop-based mode. *IEEE Transactions on Smart Grid*, 10(5):5032–5045.

Wang, P., Wang, W., and Xu, D. (2018). Optimal Sizing of Distributed Generations in DC Microgrids With Comprehensive Consideration of System Operation Modes and Operation Targets. *IEEE Access*, 6:31129–31140.

Wu, R. and Sansavini, G. (2021). Active distribution networks or microgrids? optimal design of resilient and flexible distribution grids with energy service provision. *Sustainable Energy, Grids and Networks*, 26:100461.

Wu, W., Tian, Z., and Zhang, B. (2017). An exact linearization method for oltc of transformer in branch flow model. *IEEE Transactions on Power Systems*, 32(3):2475–2476.

Yamashita, D. Y., Vechiu, I., and Gaubert, J.-P. (2020). A review of hierarchical control for building microgrids. *Renewable and Sustainable Energy Reviews*, 118:109523.

Yuan, Z. and Hesamzadeh, M. R. (2018). Second-order cone ac optimal power flow: convex relaxations and feasible solutions. *Journal of Modern Power Systems and Clean Energy volume*, 7.

Zhu, J. (2002). Optimal reconfiguration of electrical distribution network using the refined genetic algorithm. *Electric Power Systems Research*, 62(1):37–42.

Zhu, J., Nacmanson, W. J., Ochoa, L. F., and Hellyer, B. (2022). Assessing the ev hosting capacity of australian urban and rural mv-lv networks. *Electric Power Systems Research*, 212:108399.

Zill, D. and Shanahan, P. (2008). *A First Course in Complex Analysis with Applications*. Jones and Bartlett Learning.